TECHNICAL REPORT RD-WS-92-6

OPTICAL MODULATION CHARACTERISTICS AND APPLICATIONS OF LIQUID CRYSTAL TELEVISIONS

James C. Kirsch
Weapons Sciences Directorate
Research, Development, and Engineering Center

MAY 1992

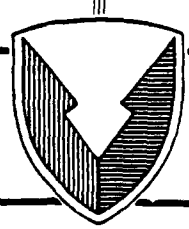

U.S. ARMY MISSILE COMMAND
Redstone Arsenal, Alabama 35898-5000

Approved for public release; distribution is unlimited.

DESTRUCTION NOTICE

FOR CLASSIFIED DOCUMENTS, FOLLOW THE PROCEDURES IN DoD 5200.22-M, INDUSTRIAL SECURITY MANUAL, SECTION II-19 OR DoD 5200.1-R, INFORMATION SECURITY PROGRAM REGULATION, CHAPTER IX. FOR UNCLASSIFIED, LIMITED DOCUMENTS, DESTROY BY ANY METHOD THAT WILL PREVENT DISCLOSURE OF CONTENTS OR RECONSTRUCTION OF THE DOCUMENT.

DISCLAIMER

THE FINDINGS IN THIS REPORT ARE NOT TO BE CONSTRUED AS AN OFFICIAL DEPARTMENT OF THE ARMY POSITION UNLESS SO DESIGNATED BY OTHER AUTHORIZED DOCUMENTS.

TRADE NAMES

USE OF TRADE NAMES OR MANUFACTURERS IN THIS REPORT DOES NOT CONSTITUTE AN OFFICIAL ENDORSEMENT OR APPROVAL OF THE USE OF SUCH COMMERCIAL HARDWARE OR SOFTWARE.

SECURITY CLASSIFICATION OF THIS PAGE

REPORT DOCUMENTATION PAGE

Form Approved
OMB No. 0704-0188

1a. REPORT SECURITY CLASSIFICATION Unclassified	1b. RESTRICTIVE MARKINGS
2a. SECURITY CLASSIFICATION AUTHORITY	3. DISTRIBUTION / AVAILABILITY OF REPORT *Approved for public release; distribution is unlimited.*
2b. DECLASSIFICATION / DOWNGRADING SCHEDULE	
4. PERFORMING ORGANIZATION REPORT NUMBER(S) Technical Report-RD-WS-92-6	5. MONITORING ORGANIZATION REPORT NUMBER(S)
6a. NAME OF PERFORMING ORGANIZATION Weapons Sciences Directorate RD&E Center 6b. OFFICE SYMBOL (*If applicable*) AMSMI-RD-WS-PO	7a. NAME OF MONITORING ORGANIZATION
6c. ADDRESS (*City, State, and ZIP Code*) Commander, U.S. Army Missile Command ATTN: AMSMI-RD-WS-PO Redstone Arsenal, AL 35898-5248	7b. ADDRESS (*City, State, and ZIP Code*)
8a. NAME OF FUNDING / SPONSORING ORGANIZATION 8b. OFFICE SYMBOL (*If applicable*)	9. PROCUREMENT INSTRUMENT IDENTIFICATION NUMBER
8c. ADDRESS (*City, State, and ZIP Code*)	10. SOURCE OF FUNDING NUMBERS PROGRAM ELEMENT NO. / PROJECT NO. / TASK NO. / WORK UNIT ACCESSION NO.

11. TITLE (*Include Security Classification*)

OPTICAL MODULATION CHARACTERISTICS AND APPLICATIONS OF LIQUID CRYSTAL TELEVISIONS

12. PERSONAL AUTHOR(S)

James C. Kirsch

13a. TYPE OF REPORT	13b. TIME COVERED	14. DATE OF REPORT (*Year, Month, Day*)	15. PAGE COUNT
Final	FROM Feb 90 TO Nov 91	1992 May 18	75

16. SUPPLEMENTARY NOTATION

17. COSATI CODES			18. SUBJECT TERMS (*Continue on reverse if necessary and identify by block number*)
FIELD	GROUP	SUB-GROUP	Liquid crystal television; spatial light modulator; amplitude modulator; phase modulation; optical correlator

19. ABSTRACT (*Continue on reverse if necessary and identify by block number*)

The spatial light modulator has long been one of the most critical components in optical information processing systems. The spatial light modulator typically limits both the speed and space-bandwidth product of the system of interest. The cost of individual modulators is also an inhibiting factor in the commercialization of optical processors. The subject of this report is the latest in an ever improving type of spatial light modulator - the liquid crystal television. The liquid crystal television was originally developed as a low cost pocket TV. Several researchers saw the potential for using these inexpensive devices and each new generation brings the promise of a modulator comparable in performance to the more traditional liquid crystal light valve and magneto-optic device at a fraction of the cost. Recent investigations into the phase modulating properties of the liquid crystal television have stimulated even more interest in the devices. Two of the best liquid crystal televisions have been investigated for use in optical computing systems and the results of these investigations are presented here. The phase and amplitude modulation characteristics of the Seiko LVD202 pocket color liquid crystal television and the Epson Crystal Image video projector have been measured. The LVD202 was capable of achieving a visibility of 0.94 in an amplitude modulating mode. The Seiko LCTV also modulates in excess of 330 degrees of phase. The Epson LCTV achieved a visibility of 0.96 in an amplitude modulating mode and was capable of modulating 336 degrees of phase. A phase-mostly joint transform optical correlator was constructed using two of the Seiko LCTVs which
(continued on page ii)

20. DISTRIBUTION / AVAILABILITY OF ABSTRACT	21. ABSTRACT SECURITY CLASSIFICATION	
☐ UNCLASSIFIED/UNLIMITED ☐ SAME AS RPT. ☐ DTIC USERS	Unclassified	
22a. NAME OF RESPONSIBLE INDIVIDUAL James C. Kirsch	22b. TELEPHONE (*Include Area Code*) (205) 876-8752	22c. OFFICE SYMBOL AMSMI-RD-WS-PO

DD Form 1473, JUN 86 *Previous editions are obsolete.* SECURITY CLASSIFICATION OF THIS PAGE

Continued from Block # 19:

performed as well as a similar amplitude modulating JTC with a much higher light efficiency. The Epson LCTV served as a phase-only input to a VanderLugt optical correlator with results similar to that of the traditional amplitude input correlator. This correlator also proved to be more light efficient than the amplitude modulating architecture. The results of these experiments as well as directions for future research efforts will be discussed in this report.

ACKNOWLEDGEMENTS

The author would like to express his appreciation to Dr. Don A. Gregory, Group Leader of the Photonics & Optical Sciences Group, Weapons Sciences Directorate, RD&E Center, for his insight and suggestions during the course of this research. The author must also thank Mr. Jeffrey A. Loudin, Mr. Tracy D. Hudson, and Ms. Cynthia Garbardi of the Weapons Sciences Directorate, for their interest, comments, and discussions regarding this work.

TABLE OF CONTENTS

LIST OF FIGURES

LIST OF FIGURES (cont'd)

LIST OF FIGURES (cont'd)

I. INTRODUCTION

A. Spatial Light Modulators

Optical information processing is a laboratory phenomena looking for applications in the "real-world" and several research facilities are actively pursuing the development of fieldable optical systems [1]. Many factors seem to be competing with this transition including the current state-of-the-art in digital information processing. The lead held by the digital industry and its research base will continue to expand unless optics can find a niche in an increasingly digital world. The biggest contributing factor to the lack of "real-world" optical systems has, in the past, been a lack of devices available to the optics community.

The era of modern optics began with the invention of the laser and, at this point, only a handful of devices, known as spatial light modulators, exist which are capable of providing real-time input to coherent optical systems. Spatial light modulators are essentially programmable incoherent to coherent information transducers. Although real-time has traditionally meant video frame rates, this definition should now be expanded to mean "as fast as the information occurs or is needed." Real-time optical interconnects, for instance, will require a spatial light modulator (SLM) capable of much faster frame rates than the TV standard 30 Hz. Most devices currently on the market will operate no faster than video (frame or perhaps field) rates.

The spatial light modulators available today can be categorized into five areas - liquid crystal devices (LCDs), deformable mirror devices (DMDs), magneto-optic devices (MODs), electro-optic devices (EODs), and acousto-optic devices (AODs). Of these modulators, only AODs have found widespread use outside the laboratory. AODs have been used in a variety of information processing systems including spectrum analyzers and synthetic aperture radars. The Hamamatsu microchannel spatial light modulator (MSLM) suffers from low resolution and low speed [2]. The latest MOD provides high contrast and a speed improvement over earlier versions but it is still a binary device [3]. The pixel count has improved from 128 x 128 to 256 x 256 but the pixel size remains the same. DMDs have the potential to solve the speed requirement but current devices suffer from low resolution (128 x 128), low visibility, and low optical efficiency [4]. They have been used in some laboratory experiments and are under investigation for use in high definition television systems but are not commercially available. The ferroelectric liquid crystal light valves (FELCs) promise high resolution, high speed, and high visibility, but most commercial devices are binary [5]. The optically addressed FELCs also suffer from low optical sensitivity. Hoescht Celanese and GEC-Marconi are marketing an amorphous silicon liquid crystal light valve (LCLV) which rivals the FELCs in resolution and offers both improved optical sensitivity and analog operation [6]. This particular LCLV will also operate at 60 Hz frame rates.

The salient characteristics for these different SLMs are shown in Table 1.1. All of the SLMs have one characteristic in common - a price tag in excess of $15,000. Although several of the devices are suitable for laboratory optical systems, none can be considered inexpensive. Most research facilities, such as universities, cannot afford to spend as much or more for the spatial light modulator than the entire rest of the optical system. A recent addition to the spatial light modulator market offers many of the same characteristics with a

marked decrease in cost. The liquid crystal television (LCTV) compares favorably with most of the spatial light modulators listed in Table 1.1 at a cost of less than $1,000 each.

B. Liquid Crystal Televisions

The liquid crystal television is based on the twisted nematic field effect (TN-FE) mode liquid crystal cell [7]. The liquid crystal material is sandwiched between two glass substrates coated with transparent electrodes as shown in Figure 1.1. The axes (or directors) of the liquid crystal molecules are oriented parallel to the substrate surfaces which are also coated with an alignment layer. The alignment layer forces a homogeneous alignment of the liquid crystal over the substrate surface. The two substrates are oriented such that the liquid crystal alignment at one surface is perpendicular to that at the other surface. This orientation induces a gradual twist in the liquid crystal material between the two surfaces. The liquid crystal sandwich is typically about 10 μm thick.

Operation of the liquid crystal cell is depicted in Figure 1.1. The gradual twist in the liquid crystal material is present in the ground state - no external electric field applied to the electrode structure. The incident light is polarized in the direction of the input polarizer which can be aligned parallel or perpendicular to the liquid crystal material. As the light propagates through the cell, the liquid crystal material acts as a polarization waveguide and the twisted structure rotates the polarization vector by 90 degrees. The output plane of polarization is then perpendicular to the transmission axis of the analyzer and all light is blocked. This phenomena occurs only if the helical pitch of the liquid crystal directors is large when compared to the wavelength. That is,

$$\Delta nd \gg \frac{\lambda}{2} \qquad (1\text{-}1)$$

TABLE 1.1. Salient Characteristics of Several Common SLMs

SLM	Visibility	Resolution	Size	Speed	Cost
MSLM	0.5	4 lp/mm	25 mm dia	2 sec	$25K
MOD	0.91	6.4 lp/mm	1 x 1 cm	200 Hz	$18K
DMD	0.50	10 lp/mm	0.64 cm	60 Hz	?
FELC	0.90	40 lp/mm	12.5 mm dia	60 Hz	$17.5K
HC LCLV	0.86	60 lp/mm	50 x 50 mm	60 Hz	$25K

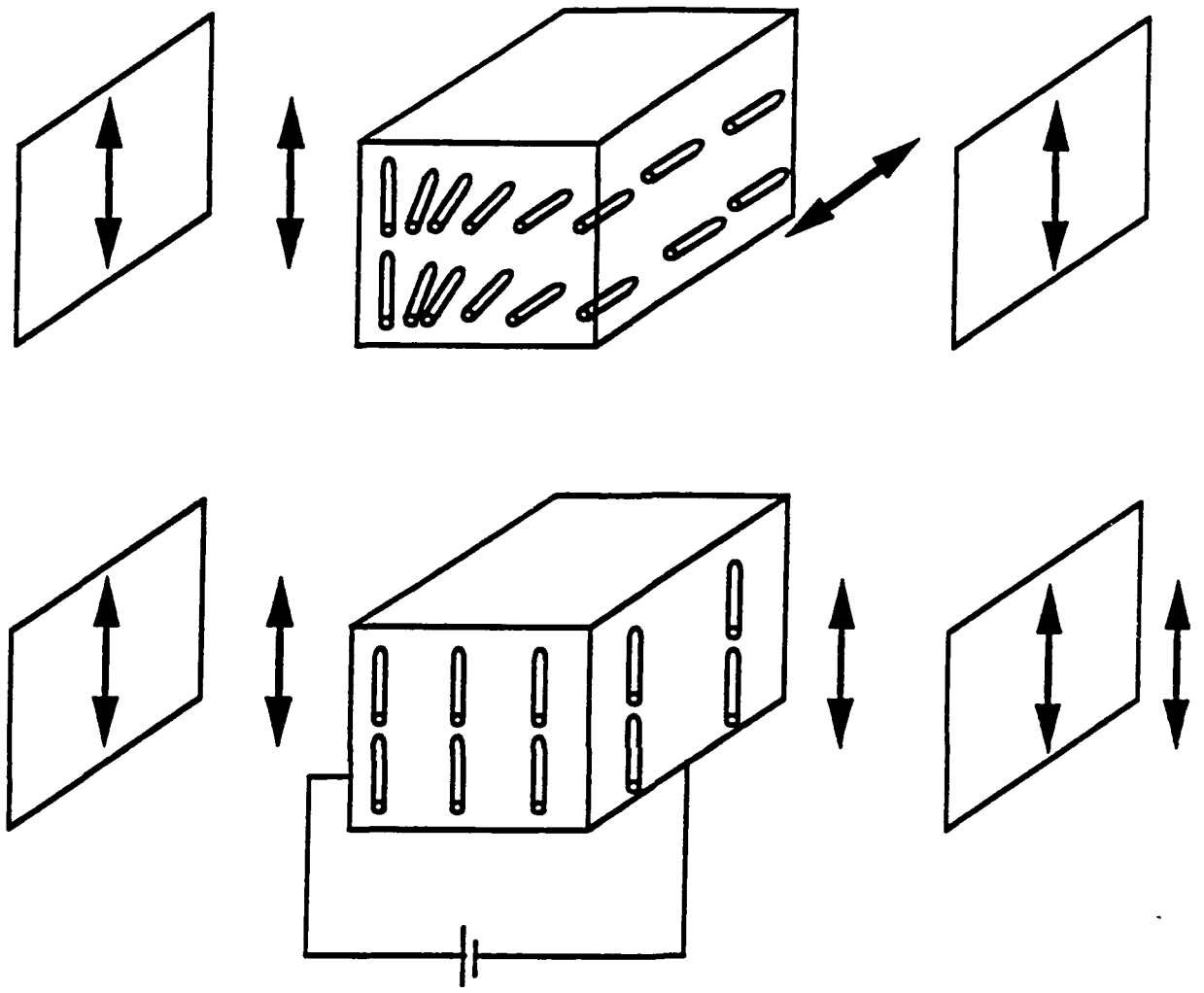

Figure 1.1. Operation of the twisted nematic field effect liquid crystal cell.

where d is the cell thickness, Δn is the refractive index anisotropy, and λ is the wavelength of the incident light [8]. The helical pitch of the liquid crystal twist is typically four times the thickness of the cell. As an example, consider a typical cell with d = 10 μm and Δn = 0.2 - 0.4. The condition is then satisfied over the entire visible wavelength range. This rotation of the plane of polarization has been measured for two different LCTVs and will be presented in later chapters.

An external electric field can be applied to switch the liquid crystal cell "on". The liquid crystal molecular directors tend to align themselves with an electric field above a certain threshold level. The amount of "untwist" experienced by the material is dependent

on the amplitude of the electric field. A strong enough field will, ideally, completely untwist the liquid crystal. Light incident on the cell undergoes no polarization rotation and emerges parallel to the analyzer's transmission axis. The light is therefore transmitted by the analyzer. The degree to which this reorientation can be accomplished will be presented for two different devices later in this report.

The structure of a liquid crystal television is shown in Figure 1.2. The intersection of the transparent row and column electrodes forms individual picture elements or pixels. Each pixel is controlled by proper selection of its row and column electrodes. A pixel is addressed when pulses traveling along the electrodes arrive at the same junction. An initial bias voltage is also placed across the entire cell to control the overall transmission of the LCTV.

The update rate of the LCTV is based on the composition of a video frame. A single video frame of approximately 525 lines consists of two interlaced fields. Each field consists of 262.5 lines. The odd field of each frame is written to the odd rows of the normal television. The even field is then written to the even rows of the television. LCTVs operate in a slightly different manner. The first 20 lines of any video field are occupied by the vertical retrace. This leaves 242.5 active lines per field. The liquid crystal television's addressing scheme drops the first and last 11 lines of the field. The remaining 220 lines are fed line by line to the pixels of the LCTV. The second field overwrites the first field line by line, so the LCTV is actually updated at a 60 Hz frame rate. Both fields use every available line of the LCTV [9].

The early LCTVs suffered from low resolution and low visibility [10,11]. The long idling time between successive addressings of an individual pixel allowed the liquid crystal to partially return to the ground state twist before the entire screen was written [12]. This problem has been solved with the addition of a thin film transistor (TFT) switch at each pixel. The TFT switch, in conjunction with the capacitance of the liquid crystal material, forces the material to remain in the desired state for longer periods of time. If the inherent capacitance of the material is insufficient to maintain the required charge, external capacitance is added to maintain the charge for the entire field time [13].

C. Phase Modulation Effects

The amplitude modulation characteristics of the LCTV are due to the twist in the orientation of the liquid crystal molecules in the sandwich structure. The twist acts as a polarization waveguide for the incident light and an output analyzer blocks on orientation of the polarization to form the amplitude image. The orientation of the liquid crystal molecular directors not only rotates, however, it also tilts. This tilt, illustrated in Figure 1.3, gives rise to a controlled birefringence in the cell which can be exploited to achieve a phase modulation [14]. This phase modulation has been discussed by several authors in the last few years [15,16,17].

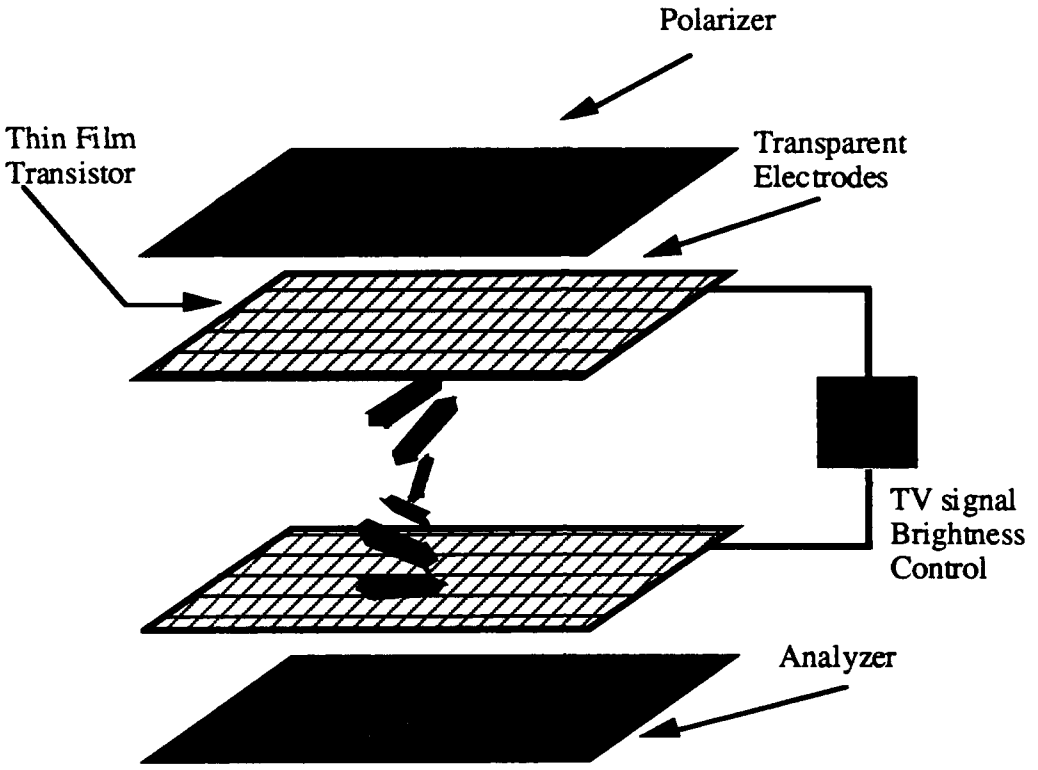

Figure 1.2. Structure of the liquid crystal television.

Consider the structure shown in Figure 1.3 when illuminated with light whose plane of polarization is parallel to the molecular director. The orientation of the molecules is shown for three different cases. As the applied voltage increases to a point above the threshold, the molecules begin to tilt as well as twist. The liquid crystal material has a positive anisotropy, i.e.:

$$n_e - n_o = \Delta n \rangle 0 \qquad (1\text{-}2)$$

and so the incident light initially sees a material with index of refraction n_e. As the tilt angle, α, tends toward 90 degrees as shown in Figure 1.3(b), the index of refraction tends toward the ordinary index of refraction of n_o. The applied voltage eventually reaches a point where the molecular directors are perpendicular to the incident plane of polarization. The amount of tilt present in a particular pixel determines the amount of birefringence the incident light will encounter. The tilt is a function of the applied voltage (bias and gray level) and gives rise to a controlled birefringence. A phase shift is then induced between light traveling through pixels with different tilt angles. The relative phase shift can be represented by:

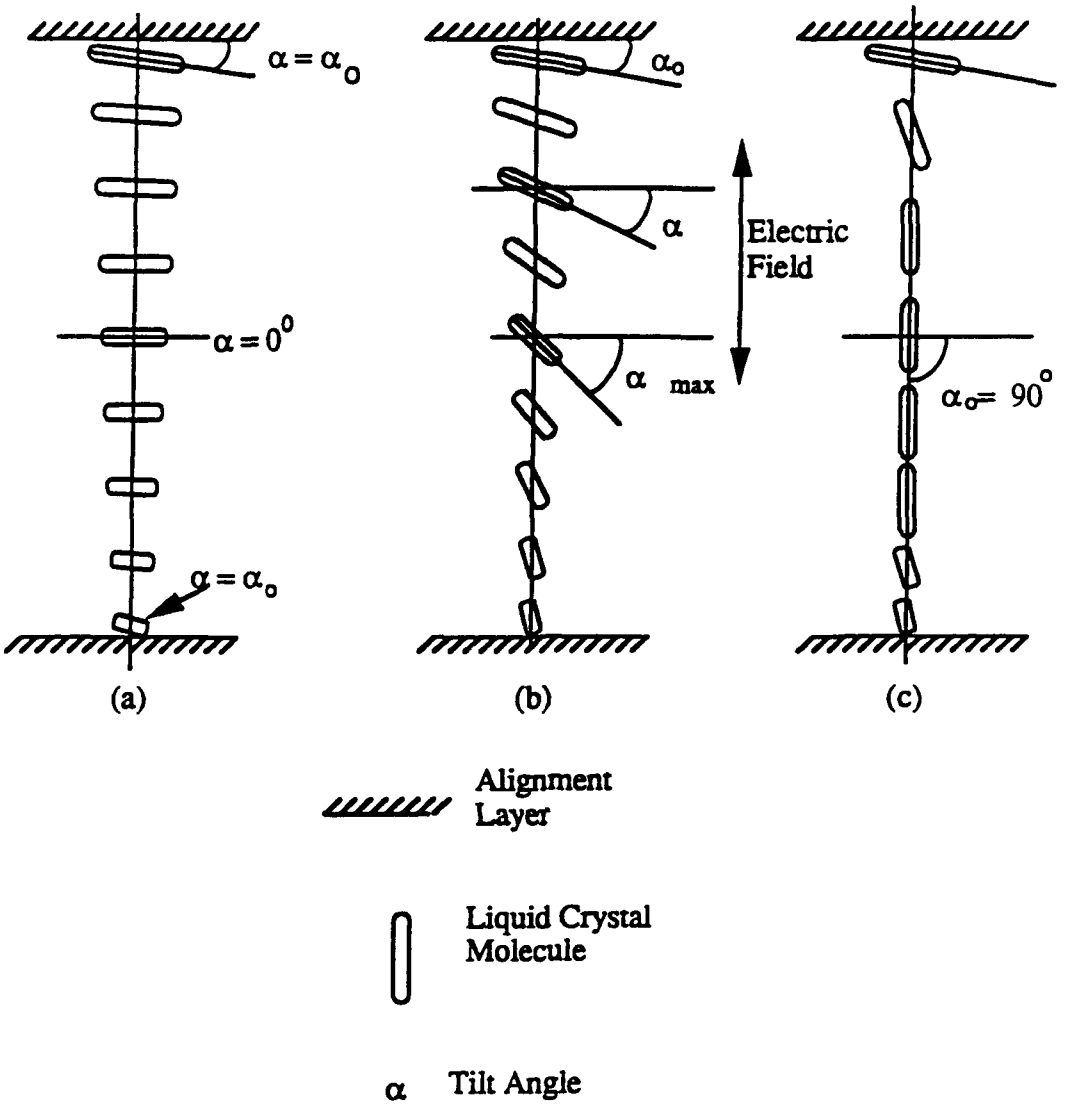

Figure 1.3. Illustration of the tilt and twist characteristics of the liquid crystal cell at (a) equilibrium, (b) a field slightly above threshold, and (c) a field well above the threshold. (adapted from Ref. 7).

$$\Delta\phi = \frac{2\pi}{\lambda} n(\alpha)\, d \qquad (1\text{-}3)$$

where $n(\alpha)$ is the index of refraction as a function of tilt angle, d is the thickness of the cell, and $\Delta\phi$ is the relative phase shift between extraordinary and ordinary rays.

Now consider Figure 1.3 with incident light whose plane of polarization is perpendicular to the molecular directors. The light sees the ordinary index of refraction. As the applied voltage increases, the molecules begin to tilt; however, the polarization remains perpendicular to the directors. The incident light, therefore, always sees the same index of refraction and no phase shift occurs.

This controllable birefringence property provides a means for encoding an image in the phase of coherent light. The incident polarization is aligned parallel to the molecular director on the front surface of the liquid crystal cell and the desired phase shift is encoded by proper choice of input gray levels. No analyzer is present on the output of the LCTV and so no amplitude information is presented to the optical system. If amplitude only modulation is desired, the input polarization can be aligned perpendicular to the molecular director and no phase modulation will be present. The amplitude information is then decoded by the output analyzer.

The hybrid phase modulation properties of the LCTV offer many exciting possibilities for applications in optical systems. The amplitude modulation characteristics rival those of the more traditional spatial light modulators and the phase modulation characteristics offer opportunities for improved light efficiency. Several architectures will be presented in this report which make use of the "phase only" modulation properties. A section of this report will also be devoted to a discussion of the possibilities for full complex modulators and an architecture for implementing such a device will be presented.

II. CHARACTERISTICS OF THE SEIKO LCTV

A. The Seiko Model LVD202 Liquid Crystal Television

The Seiko LVD202 was perhaps the best LCTV on the market prior to the advent of the Epson and Sharp video projectors. One of the first applications of the Seiko LCTV was in a joint transform optical correlator [18]. This particular LCTV offered several advantages over its predecessors not the least of which was the relative flatness of the screen itself. Previous LCTVs were typically immersed in liquid gates before insertion into an optical system [11]. The LVD202 had a sufficiently good surface quality to avoid this inconvenience. A photograph of the Seiko LCTV is shown in Figure 2.1.

The Seiko LCTV consists of 240 columns x 220 rows of pixels on a 2" diagonal screen. A photograph of the pixel structure is shown in Figure 2.2. The far field diffraction pattern due to this pixel structure is shown in Figure 2.3. Each pixel measures 155 μm x 120 μm with a center-to-center spacing of 162.5 μm x 132.5 μm. The LVD202 is a color television and as such uses color filters over the liquid crystal sandwich. The filters are arranged such that like color pixels run along the diagonal. Three LCTV pixels are required to form one color image pixel. The net effect of these color filters when the LCTV is used with monochromatic light is a resolution reduction of 3:1. Assuming that the square holes in the color filter are active, the total active area of the LCTV is 86.4 percent (28.8 percent for each color) with a transmission efficiency at 0.6328 μm of 28 percent.

The video addressing of an LCTV was described in Chapter 1. One difference noted in the Seiko LCTV was the orientation of the input and output polarizers. Typically

LCTV polarizers are oriented with their transmission axes parallel. A bright portion in the video signal then corresponds to a voltage applied to the liquid crystal sandwich to align the molecular directors and reduce the amount of twist. The brighter the video signal, the more voltage applied, and hence the amount of twist is decreased. The Seiko LCTV used crossed

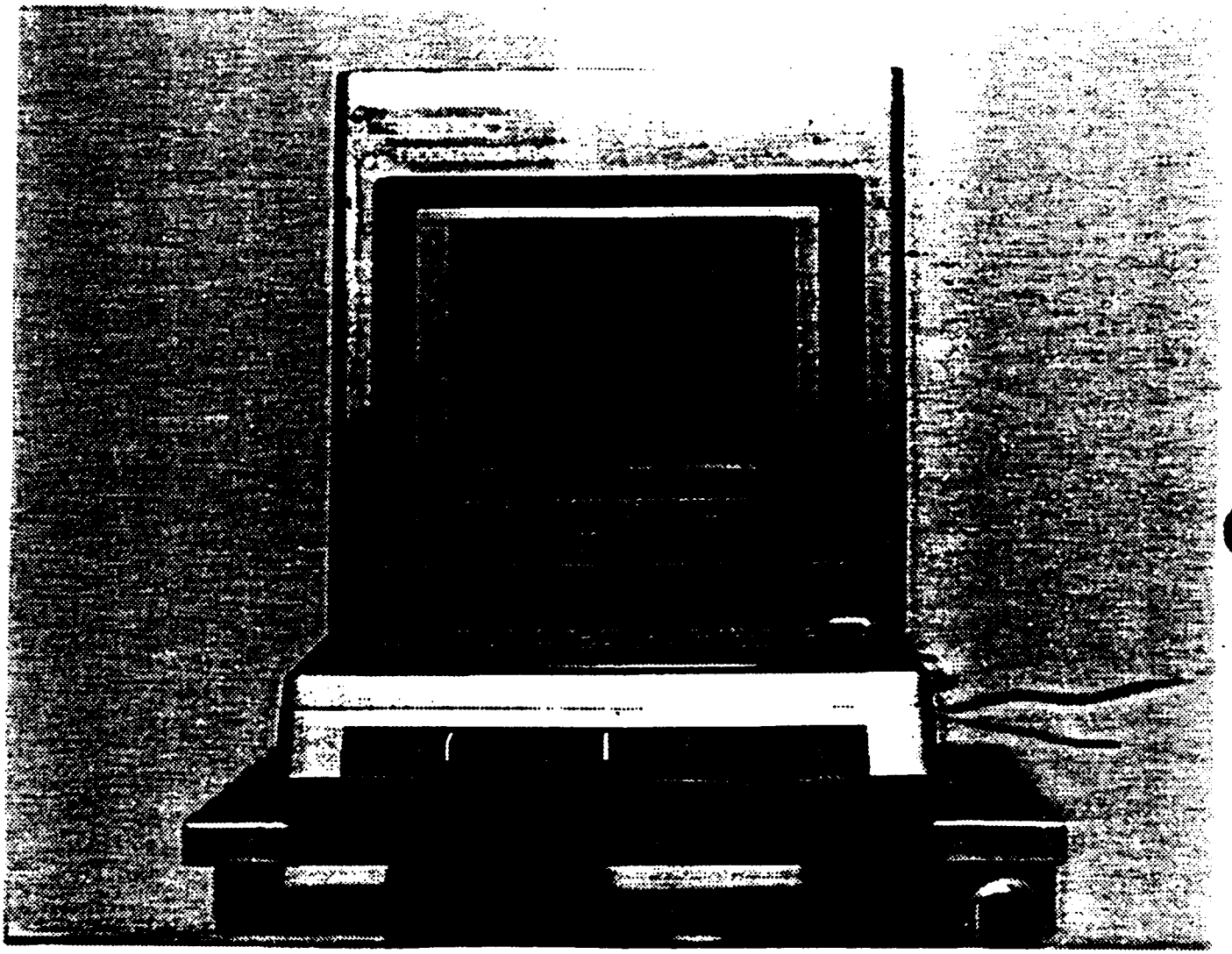

Figure 2.1. Photograph of the Seiko LVD202 LCTV.

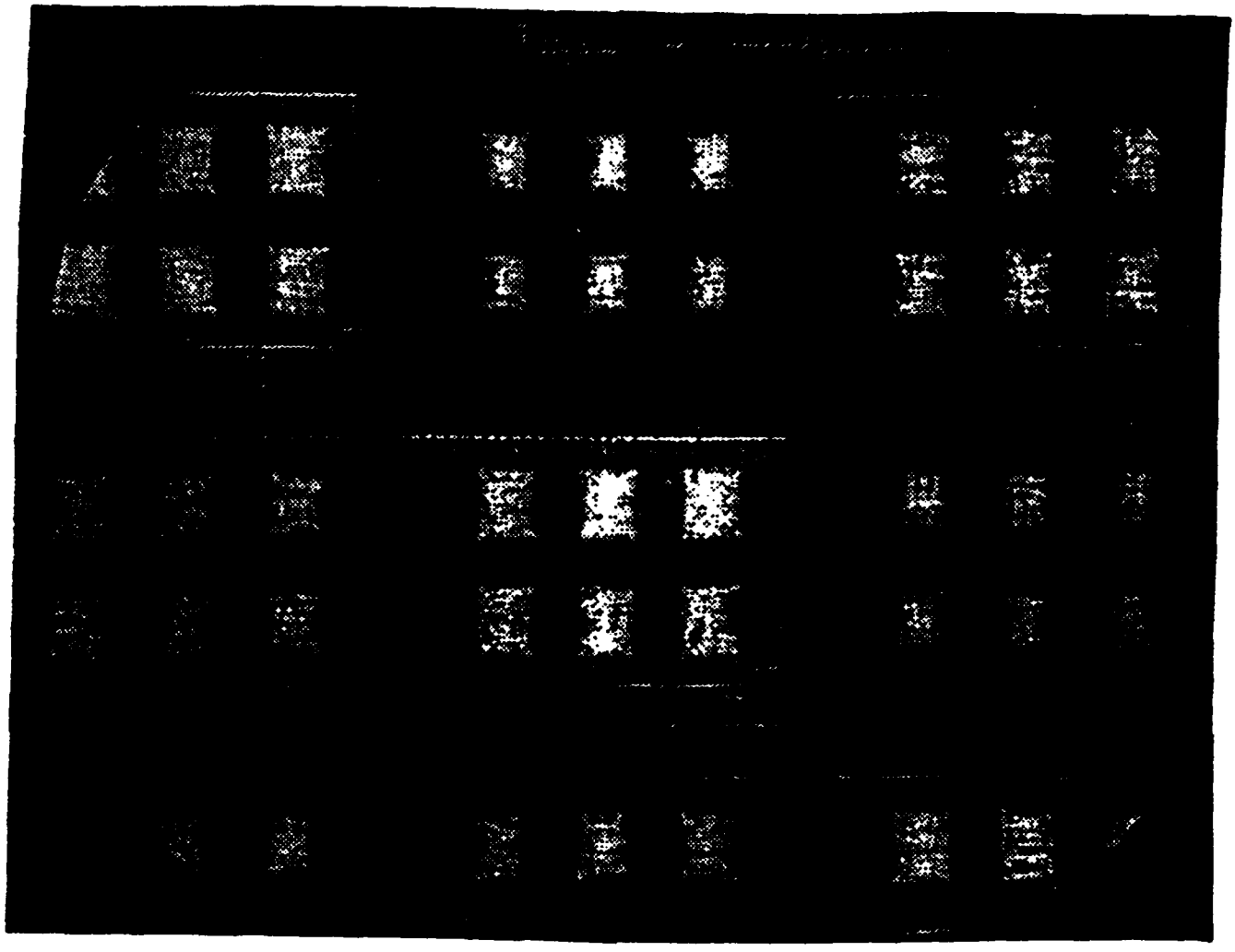

Figure 2.2. Photograph of the Seiko LVD202 pixel structure.

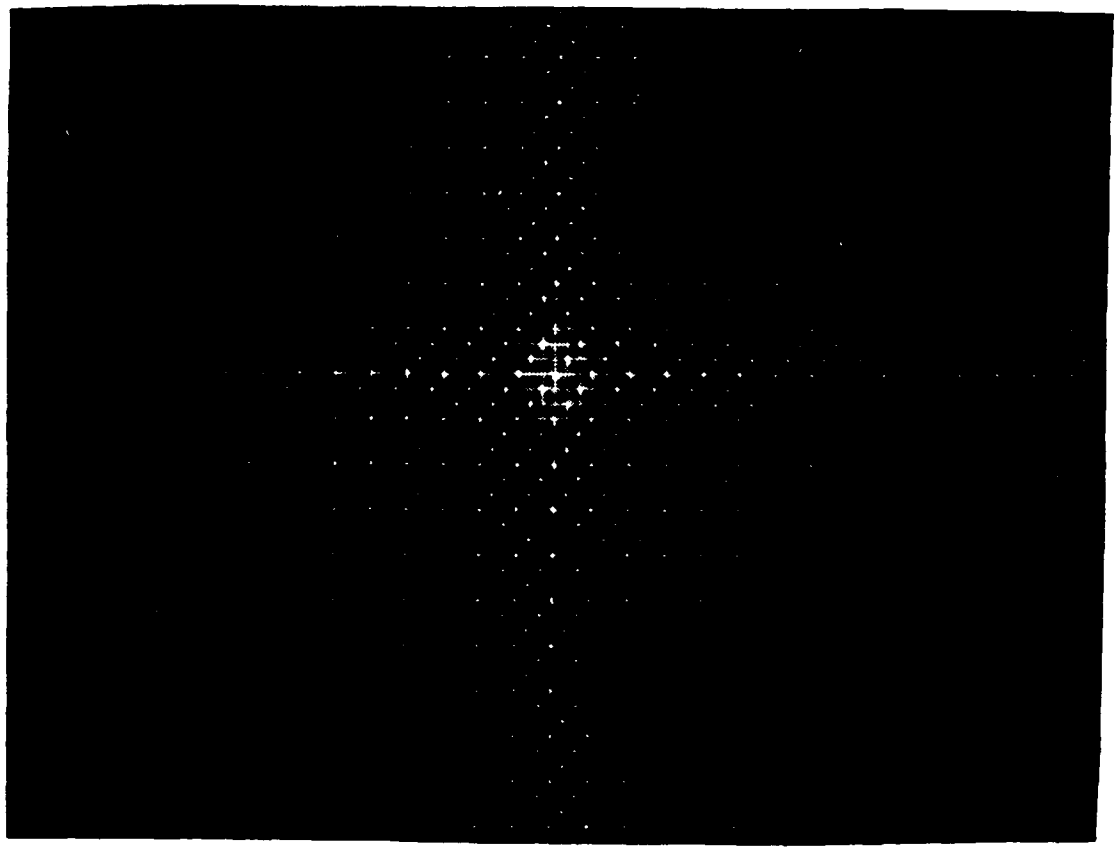

Figure 2.3. Photograph of the far field diffraction pattern due to the pixel structure.

polarizers. A maximum in the video signal then corresponded to a minimum voltage applied to the liquid crystal cell. This phenomena was first reported by Tam at Penn State University [19].

B. Visibility

One of the most common parameters quoted when discussing spatial light modulators is the contrast ratio. The contrast ratio is defined as:

$$C = \frac{I_{max}}{I_{min}} \qquad (2\text{-}1)$$

where I_{max} and I_{min} are the intensities measured for a fully "on" pixel and a fully "off" pixel, respectively, and C is the contrast ratio. The contrast ratio, therefore, has a lower bound of

0 but no upper bound. This is not an effective means for comparing the modulation properties of different spatial light modulators. Consider a device with a contrast ratio of 50:1. It is hard to judge how much improvement is made by increasing the contrast to 100:1. It is even harder to compare this number to a device with a contrast ratio of 1000:1. A much more effective metric for comparing two devices is to compare visibilities. Visibility, as defined by Michelson, is given as [20]:

$$V = \frac{I_{max} - I_{min}}{I_{max} + I_{min}} . \qquad (2\text{-}2)$$

The visibility is limited to values between 0 and 1.0 with 0.8 considered to be a good value. Using the previous examples, C = 100 corresponds to V = 0.98, C = 50 corresponds to V = 0.96, and C = 1000 corresponds to V = 0.998. Comparing the numbers for visibility, it can be seen that all three devices have very high visibilities with only a small gain between even C = 50 and C = 1000. An argument can be made, however, that the contrast ratio is a more meaningful quantity when discussing optical computing applications. Visibility is essentially a measure of the imaging quality of an optical system or component. The nature of the visibility measurement tends to suppress the dynamic range information contained in the measurements of the brightest and darkest portions of the signal. Contrast ratio, however, preserves this information and, for this reason, will also be reported in this report.

The optical system used for the visibility measurements is shown in Figure 2.4. A pattern of eight alternating fully "on" and fully "off" bars was displayed on the LCTV. The (0,0) order of the Fourier transform of the LCTV (which is calculated for the Epson LCTV in the Appendix) was imaged onto a Pulnix model 840 CCD camera. The output of the camera was fed through a Colorado Model 321 video analyzer and displayed on a monitor. The output of the video analyzer was recorded on a chart recorder. Several scans were made through the bars to determine the relative intensities of the black and white bars. The average visibility measured for the Seiko LCTV was 0.94 (contrast ratio of 33:1). A photograph of an image encoded in coherent light by the LCTV is shown in Figure 2.5. It should be noted that this one measurement does not fully characterize the visibility characteristic of the LCTV. The only way to completely characterize a spatial light modulator or any other component in an optical system is to measure its visibility versus spatial frequency modulation properties and determine the modulation transfer function. The measurement presented here is simply a reference point for later discussions.

The brightness setting on the LCTV was adjusted to provide the darkest black in the previous measurements. Measurements were also made to determine the amount of transmitted light as a function of this brightness, or bias, voltage. The optical system shown in Figure 2.3 was modified by replacing the CCD camera with a Newport Model 882 photodetector with a Model 835 power meter. The transmission axes of the two polarizers were aligned to be parallel with each other and with the vertical axis of the LCTV. A two bar pattern (fully "on" and fully "off") was displayed on the LCTV and reimaged onto the photodetector. A mask was placed on the photodetector to block the fully "on" bar. The power meter reading was recorded for various bias voltages over the full range of the brightness knob. The procedure was repeated with the fully "off" bar blocked and the fully "on" bar illuminating the detector. A plot of the power meter reading as a function of bias voltage for each bar is shown in Figure 2.6. This plot corresponds very well with a similar plot presented in the literature [21].

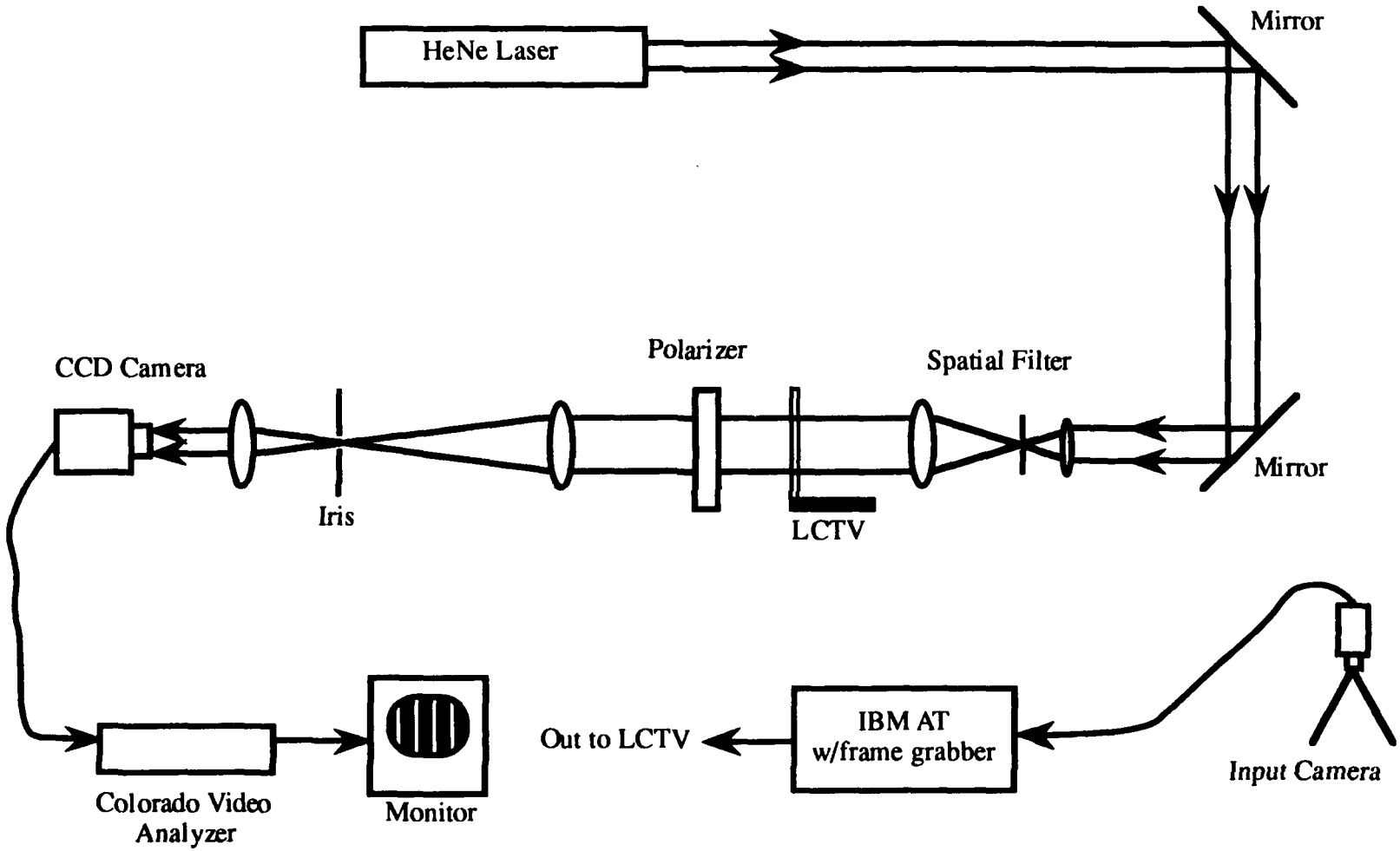

Figure 2.4. Optical system for measuring visibility.

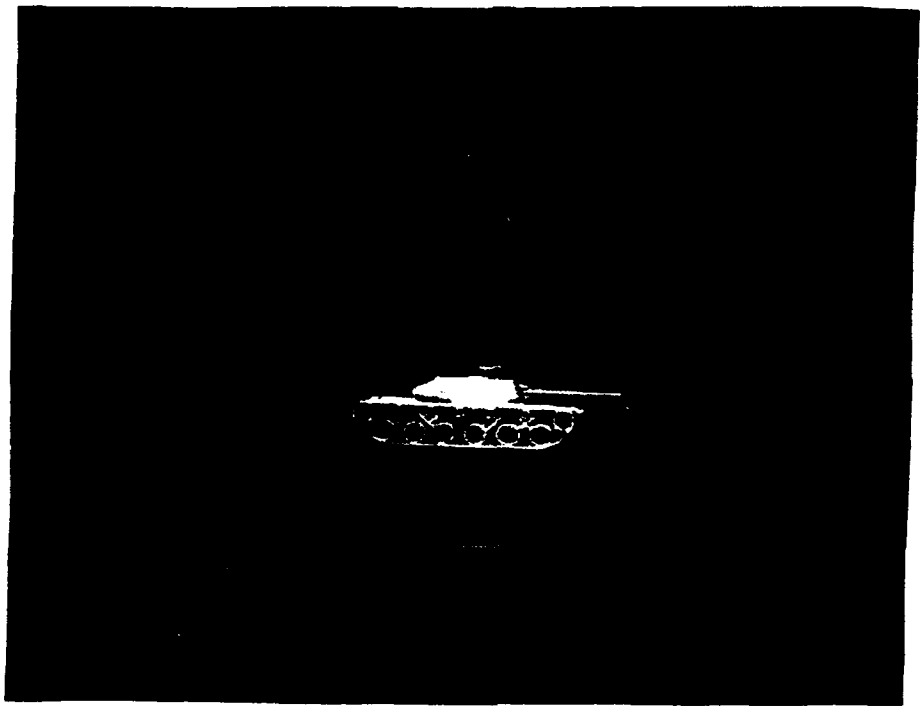

Figure 2.5. Photograph of the image encoded in coherent light by the Seiko LVD202.

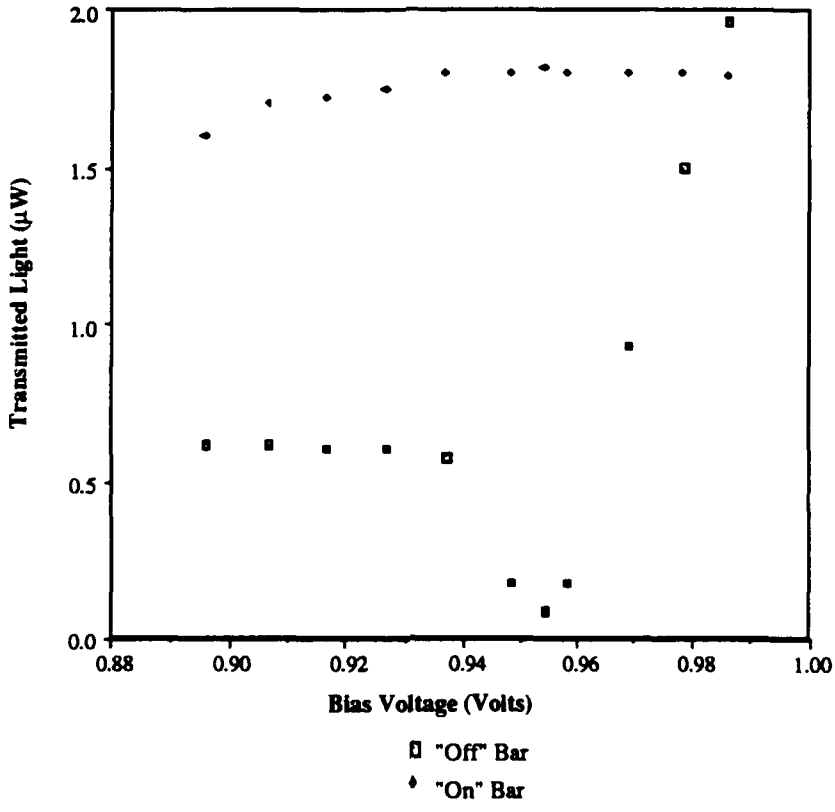

Figure 2.6 Transmitted light vs. bias voltage for the Seiko LVD202.

C. Phase Modulation

A Mach-Zehnder interferometer was used to investigate the phase modulation properties of the Seiko LVD202 LCTV. Phase modulation offers some attractive advantages such as increased transmission efficiency and the ability encode analog, rather than binary or ternary, phase filters. The phase modulation present in the LCTV can be isolated from the amplitude modulation to some degree with the proper choice of brightness setting and input video amplitude.

The Mach Zehnder interferometer is shown in Figure 2.7. Coherent illumination was provided by a HeNe laser. One leg of the interferometer serves as the reference while the other leg contains the LCTV. A half-wave plate was used to align the

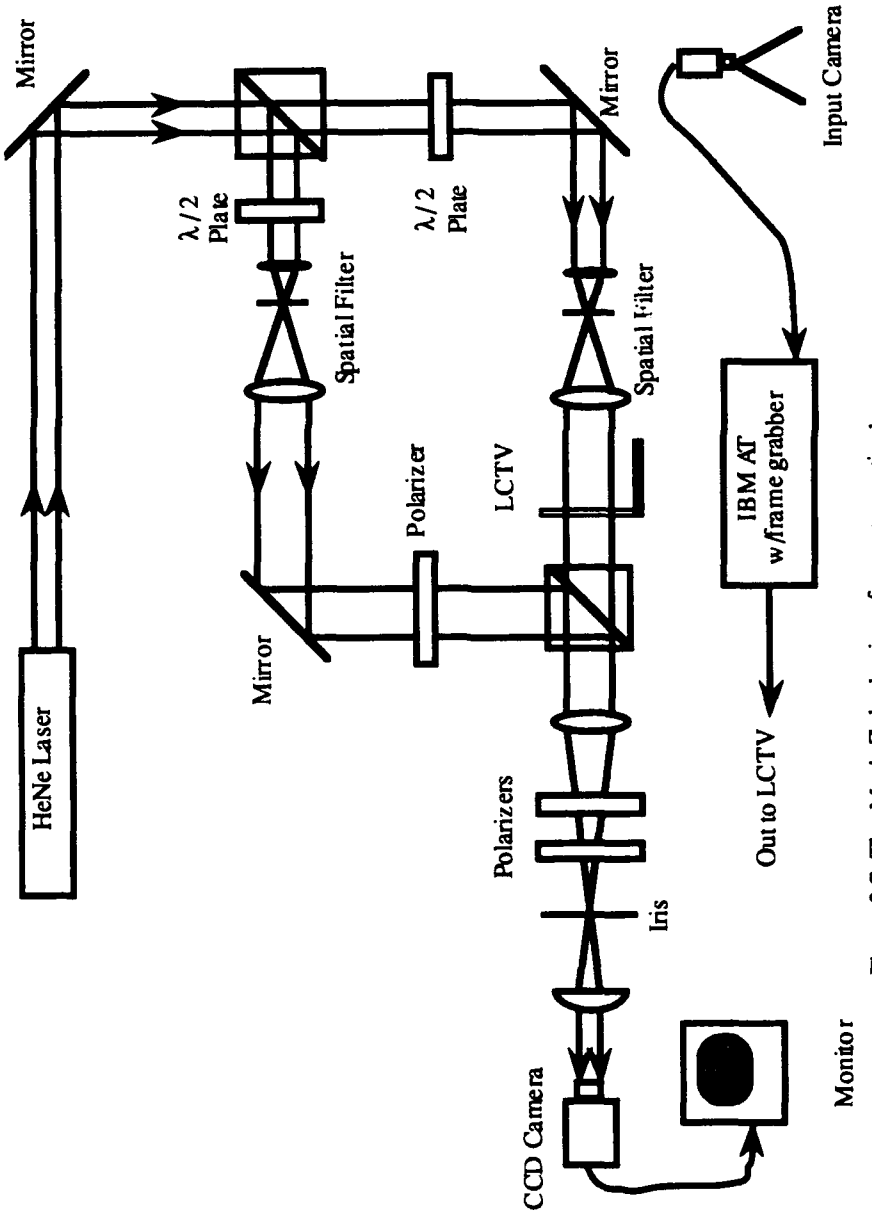

Figure 2.7 The Mach-Zehnder interferometer optical arrangement.

polarization of the incident light with the molecular director on the input side of the LCTV. The same series of eight fully "on" and fully "off" bars was displayed on the LCTV and the (0,0) order imaged onto the CCD camera. A phase difference between the fully "on" and fully "off" portions of the LCTV was characterized by an interference fringe shift at the boundary between adjacent bars. The relative phase shift was determined by measuring the amount of shift present and dividing by the separation between two adjacent fringes. The ratio of the fringe shift to the fringe separation represents the phase shift as a fraction of 2π. The maximum phase shift between a fully "on" and fully "off" section was measured to be 1.84π or 331 degrees. A photograph of the fringe structure with all pixels fully "off" is shown in Figure 2.8 while a photograph of the maximum fringe shift is shown in Figure 2.9. The phase shift as a function of bias voltage is plotted in Figure 2.10.

D. LCTV Update Rate

The addressing scheme used in most liquid crystal televisions was discussed in Chapter 1 of this report and has been verified for the Seiko LVD202 LCTV. A video multiplexing circuit was constructed which accepts two inputs and provides one output. The output video signal alternates between the two inputs at either field (60 Hz) or frame (30 Hz) rates.

The update rate of the LVD202 was verified using the optical system in Figure 2.11. Two NEC Model Ti22 CCD cameras provided slightly differing views of a single spoke wheel target. The two video signals served as the inputs to the multiplexing circuit and the output was sent to a monitor. The two cameras were adjusted so that the spoke wheel pattern in the second cycle of the multiplexer appeared to the side of the spoke wheel pattern in the first cycle as displayed on the monitor. The multiplexer output was then fed to the LCTV. Both spoke wheel patterns would be visible on the LCTV only if both cycles of the multiplexer output were sent to the liquid crystal sandwich by its drive electronics. If only every other cycle was sent to the modulator, only one spoke wheel would appear on the LCTV. The video signal displayed on the LCTV was encoded onto coherent laser light and reimaged on a Pulnix Model 840 CCD camera. Figure 2.12 is a photograph of the scene encoded by the LCTV with the multiplexer switching at 60 Hz, i.e., video field rates. As both images were visible in coherent light, the LVD202 must have been switching at field rates as described in Chapter 1.

E. Polarization Effects

Most applications of the LCTV involve its amplitude modulating properties. The amount of amplitude modulation, i.e., the maximum contrast ratio, is a function of the polarization rotation achieved by the liquid crystal. The ideal amount of rotation is 90 degrees such that the "on" and "off" states are orthogonal to each other. If this rotation is achieved, essentially all of the "on" state light is transmitted by the output analyzer while all of the "off" state light is blocked.

Figure 2.8. Photograph of the fringe structure with all pixels set to 0.

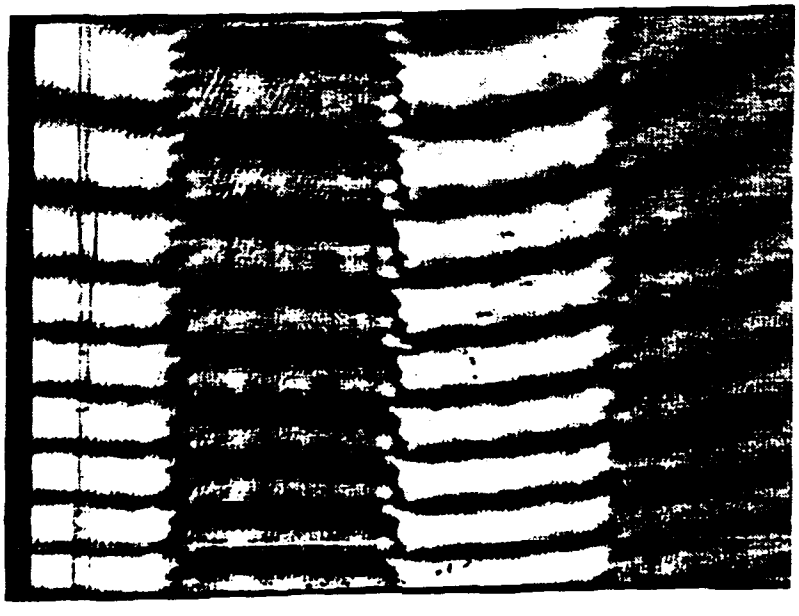

Figure 2.9. Photograph of the fringe structure with the bar pattern on the LCTV.

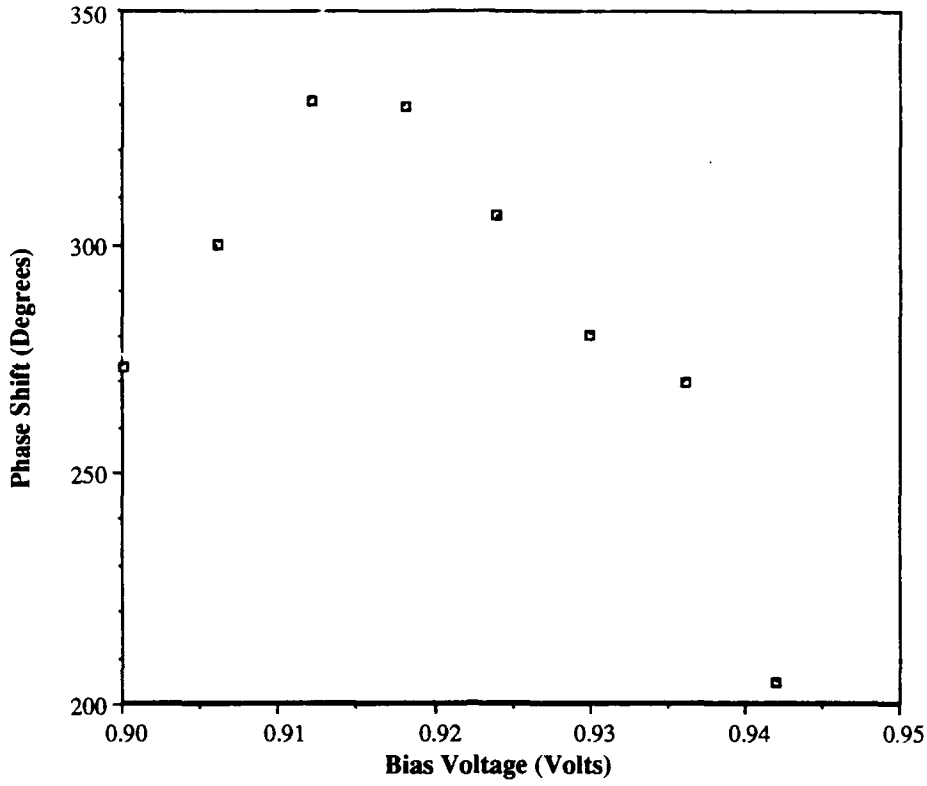

Figure 2.10. Phase shift vs. bias voltage for the Seiko LVD202 LCTV.

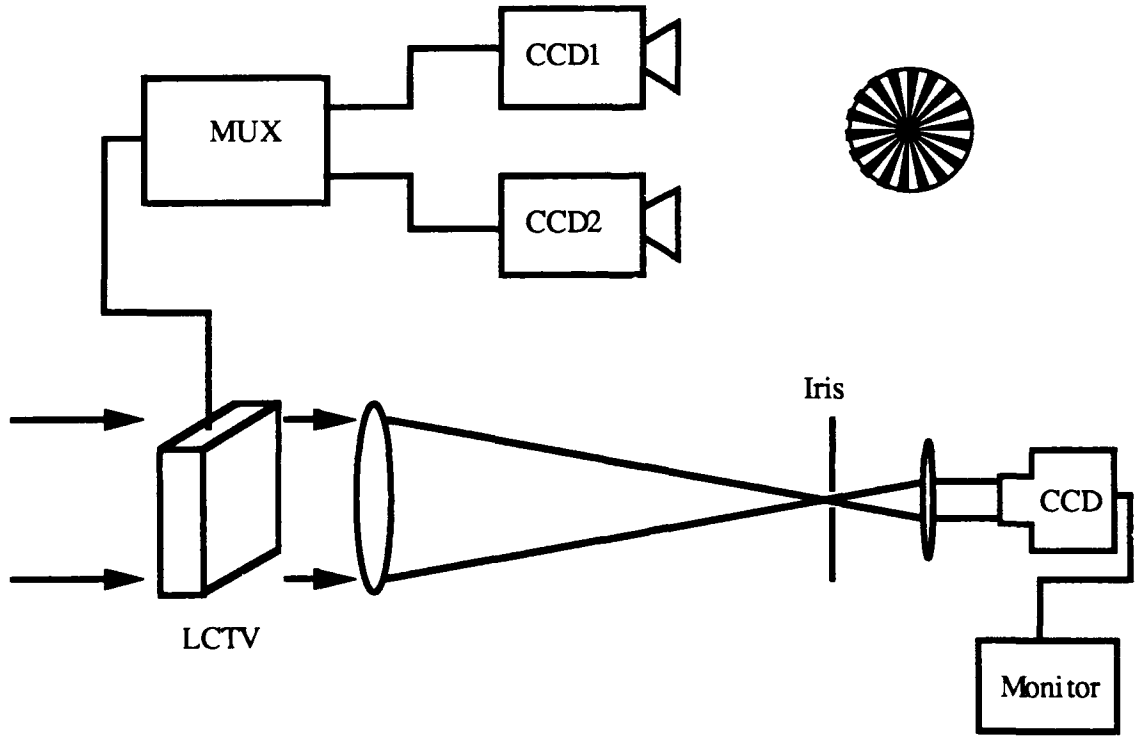

Figure 2.11. Architecture used to measure the LCTV update rate.

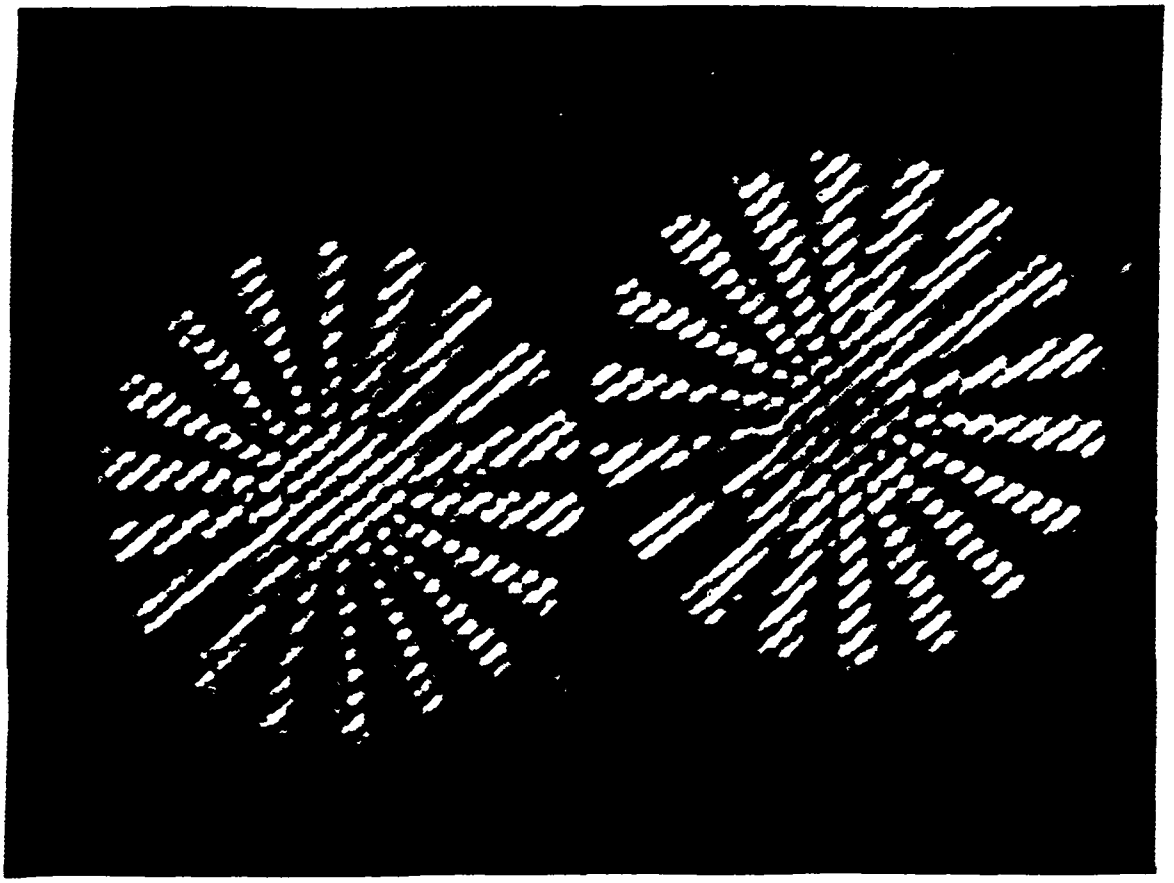

Figure 2.12. Photograph of the image encoded in coherent light by the Seiko LCTV with the multiplexer switching at field rates (60 Hz).

The optical system used to measure the polarization rotation achieved by the LCTV is similar to the system in Figure 2.4. The CCD camera was replaced with the photodetector described earlier and a scene consisting of one fully "on" and one fully "off" bar was displayed on the LCTV. The input polarizer was adjusted to transmit light linearly polarized at 0 degrees with respect to the vertical axis. The output analyzer was initially aligned parallel with the input polarizer. A mask was placed over the photodetector to block the fully "off" bar of the pattern. The output analyzer was rotated to achieve the maximum reading on the power meter for several values of the brightness voltage. The mask was then adjusted to pass only the full "off" bar and the measurements repeated. A plot of the data is shown in Figure 2.13. The vertical axis is labeled in degrees where 360 degrees is parallel to the input polarization. It can be seen that a 90 degree rotation is achieved at a brightness voltage of approximately 0.954 volts. This is also the voltage at which the maximum contrast occurs in Figure 2.6. The results in Figures 2.6 and 2.13 compare favorably with the results presented by Tam for his Seiko LVD202 [22].

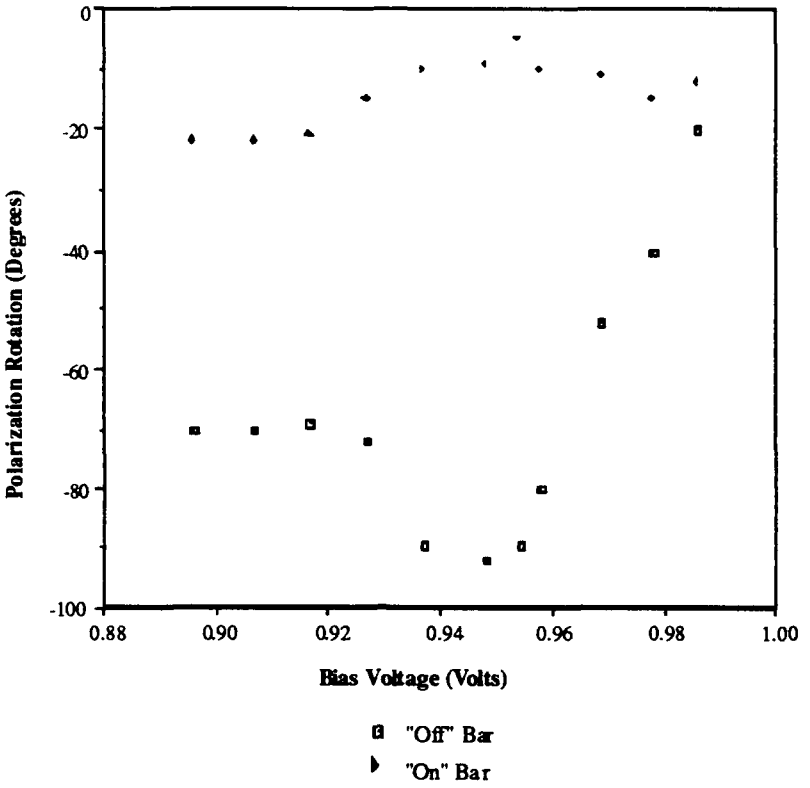

Figure 2.13. Polarization rotation vs. bias voltage for the Seiko LCTV.

III. CHARACTERISTICS OF THE EPSON LCTV

A. The Crystal Image Video Projector

More and more uses are found for LCTVs as the state-of-the-art keeps improving. The first LCTVs were low resolution low contrast devices suitable only for individual viewing under certain ambient light conditions. Gregory [23], however, was able to take even these early devices and make use of their light modulating properties in an optical system. The introduction of active matrix addressing and improvements in both semiconductor and liquid crystal technology have resulted in large displays for both television and computer monitor applications. Recently, Epson and Sharp have begun marketing portable video projectors based on small, high resolution, high contrast liquid crystal televisions.

The Epson Crystal Image video projector is shown in Figures 3.1 and 3.2. The video projector consists of three main components - the white light bulb, the optical head assembly, and the drive electronics. The optical head assembly, which is hidden underneath the printed circuit card on the lower right side of the projector in Figure 3.2, consists of three liquid crystals displays (LCDs), 2 dichroic mirrors, a custom beamsplitter, and a projection lens. The projector is capable of accepting three different video standards: National Television Systems Committee (NTSC), analog red-green-blue (RGB), and digital RGB.

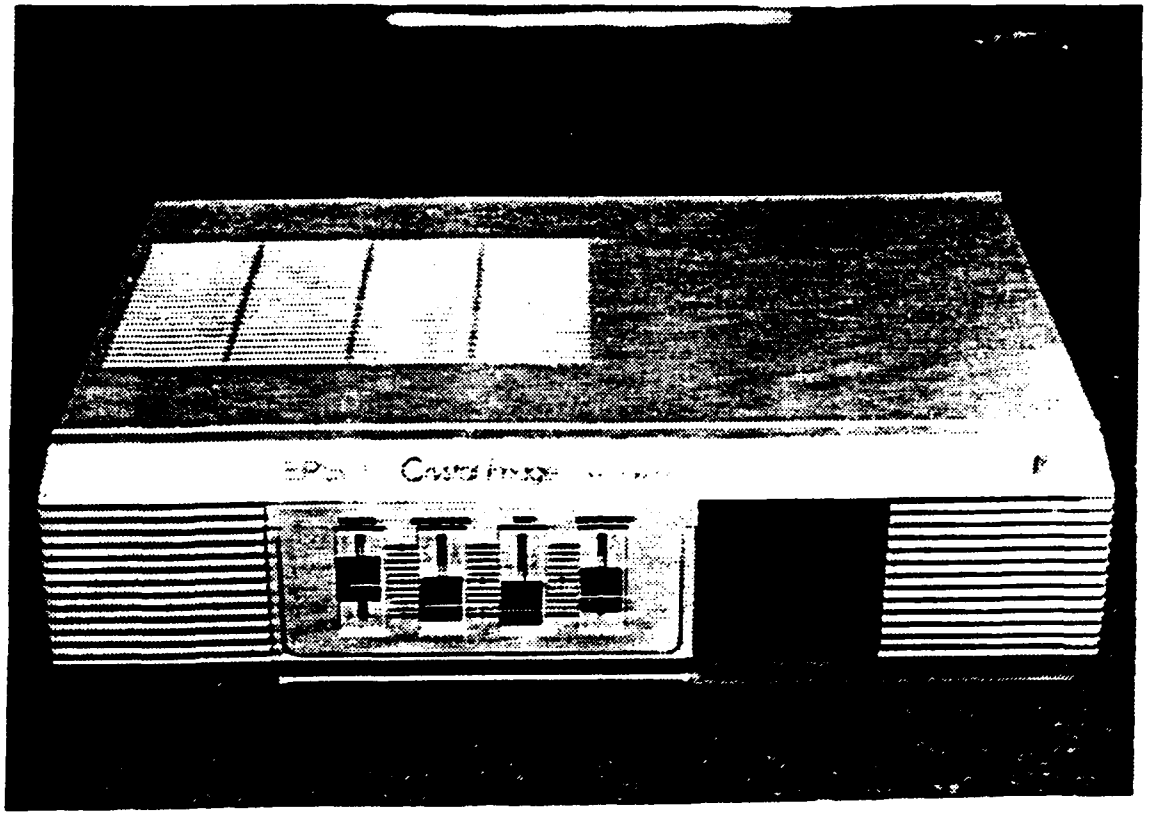

Figure 3.1. Photograph of the Epson Crystal Image video projector.

The input video standard is selected by means of a switch on the rear panel of the projector housing. The drive electronics separate the three color components (red, green, and blue) and send the separate signals to the individual LCD drivers.

The optical arrangement of the Epson video projector is shown in Figure 3.3. A high intensity projector bulb provides the white light illumination for the optical head assembly. Two dichroic dielectric mirrors split the white light into its red, green, and blue components which illuminate the three pixelated LCDs. The three components are recombined after passing through the corresponding LCD using the custom beamsplitter. The compound lens then projects the image onto the desired viewing surface.

B. The Liquid Crystal Displays

The three liquid crystal displays in the video projector are used to encode the red, green, and blue components of the color video signal into the incident projector light. Each LCD is a monocolor device illuminated by essentially monochromatic light. The red, green, and blue components are recombined by the beamsplitter to form the desired color image. The term monocolor, as applied to these displays, refers to the fact that each display in the Epson projector modulates only one color of light at a time. The color pocket LCTVs, such as the Seiko LVD202 discussed earlier, use color filters to modulate the entire color image

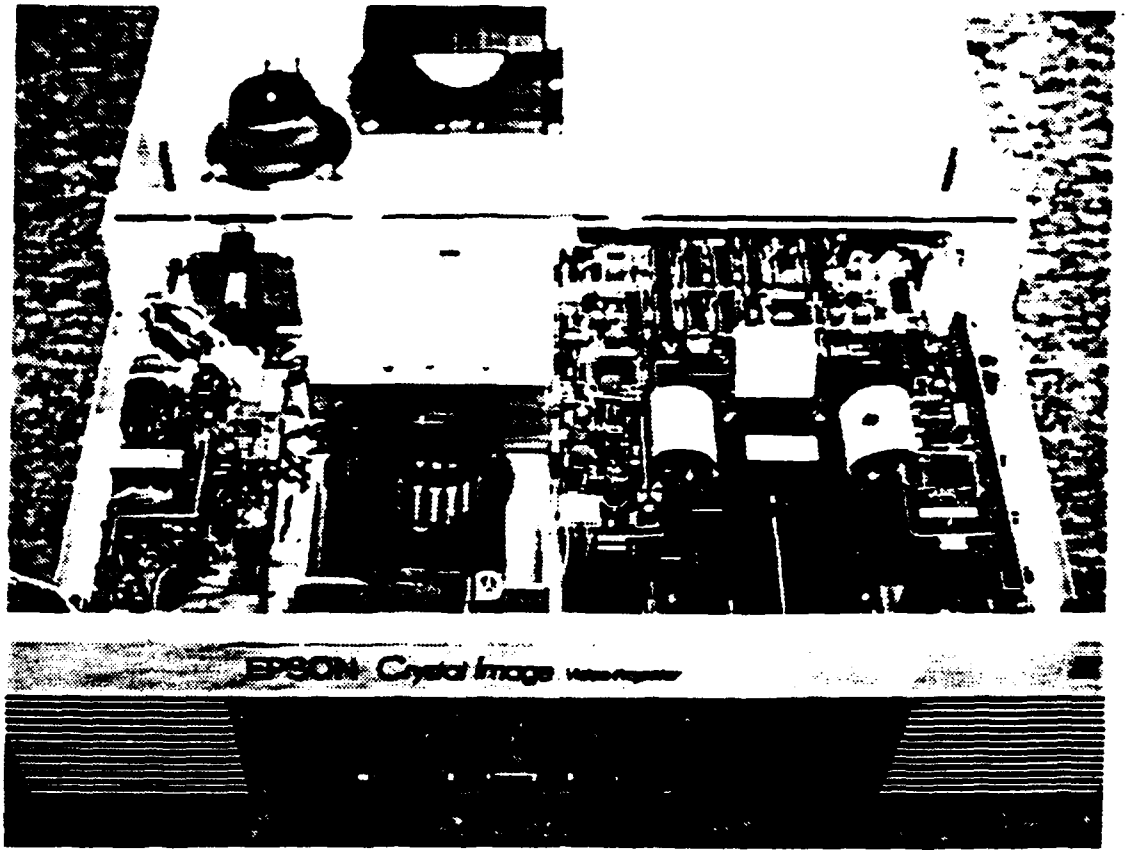

Figure 3.2. Photograph of the Epson Crystal Image video projector with the cover removed.

on one device simultaneously. This is an important advantage for the Epson liquid crystal devices in that every pixel in the display is used to modulate only one wavelength. In the color LCTVs, it takes three "subpixels" to form one image pixel. The result is essentially a 3 to 1 resolution advantage for the Epson monocolor LCDs over a color LCTV with the same total number of pixels.

A photograph of one of the Epson LCDs is shown in Figure 3.4. The dichroic mirrors ensure linear polarized light illuminates the display in the projector and an external sheet polarizer serves as the analyzer. The polarizers provided with the projector were replaced with high quality Ealing polarizers when used in the optical processing systems discussed here. The short, 23 conductor, flat lead cable connecting the display to the drive electronics was also replaced using a longer ribbon cable.

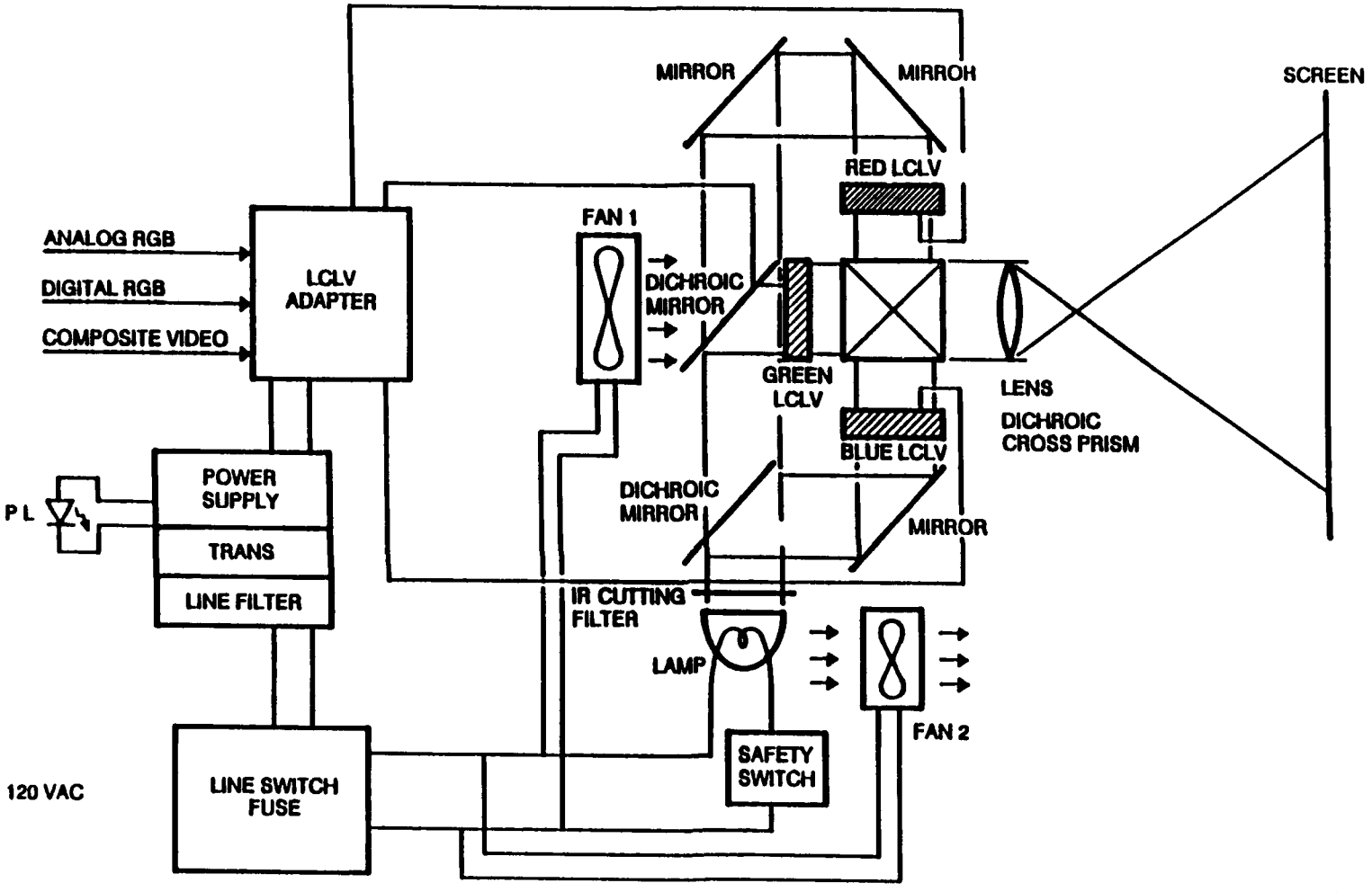

Figure 3.3. Optical arrangement of the Epson Crystal Image video projector (adapted from the Epson technical manual).

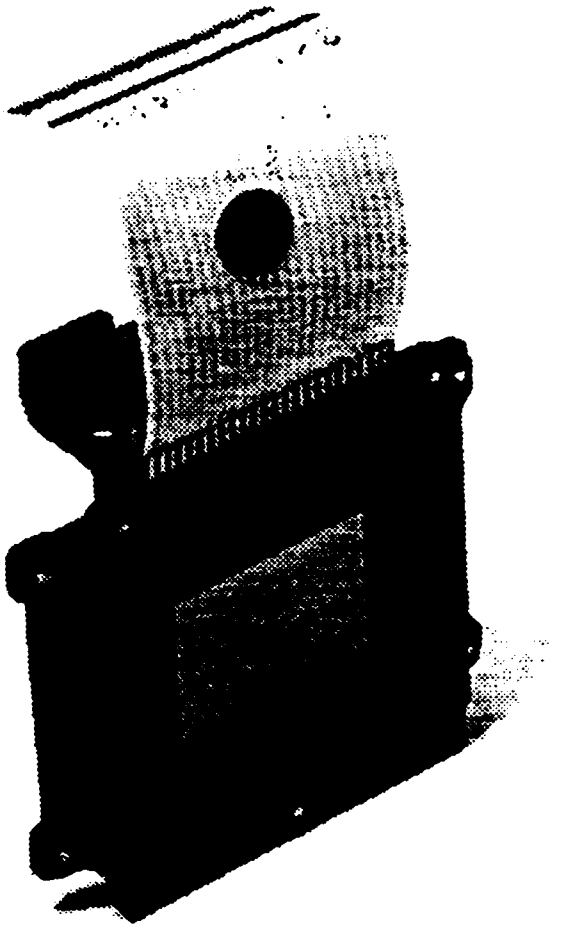

Figure 3.4. Photograph of an individual Epson LCD.

The pixel count of each LCD is 320 x 220 with a 1.25" diagonal clear aperture. Each pixel measures 60 μm x 55 μm with a center-to-center spacing of 90 μm x 80 μm. A photograph of the pixel structure is shown in Figure 3.5. The pixel pitch of the Epson LCD corresponds to a 46 percent active area. The total transmission efficiency of the device is 43 percent. A photograph of the far field diffraction pattern due to the pixel structure is shown in Figure 3.6.

C. Visibility

The visibility measurements for the Epson LCD were made in much the same manner as those for the Seiko LCTV. The optical system is shown again in Figure 3.7 for easy reference. The alternating series of fully "on" and fully "off" bars was displayed on the LCD and the (0,0) order of the Fourier transform reimaged onto the Pulnix camera. Several scans were made through the bars using the Colorado video analyzer to determine the relative intensities of the black and white bars and it was found that the white bars were saturating the camera. A neutral density (ND) filter with a transmission of 10.3 percent was required to reduce the white intensity to a level below camera saturation. At this point, however, the black bars were below the camera's sensitivity level. Several scans were made to determine the white levels. The ND filter was removed and scans made through the same areas to determine the corresponding black levels. The effects of the ND filter were taken into account and an average visibility determined. The average visibility measured for the Epson LCD was 0.96 (contrast ratio of 49:1). Again, this measurement

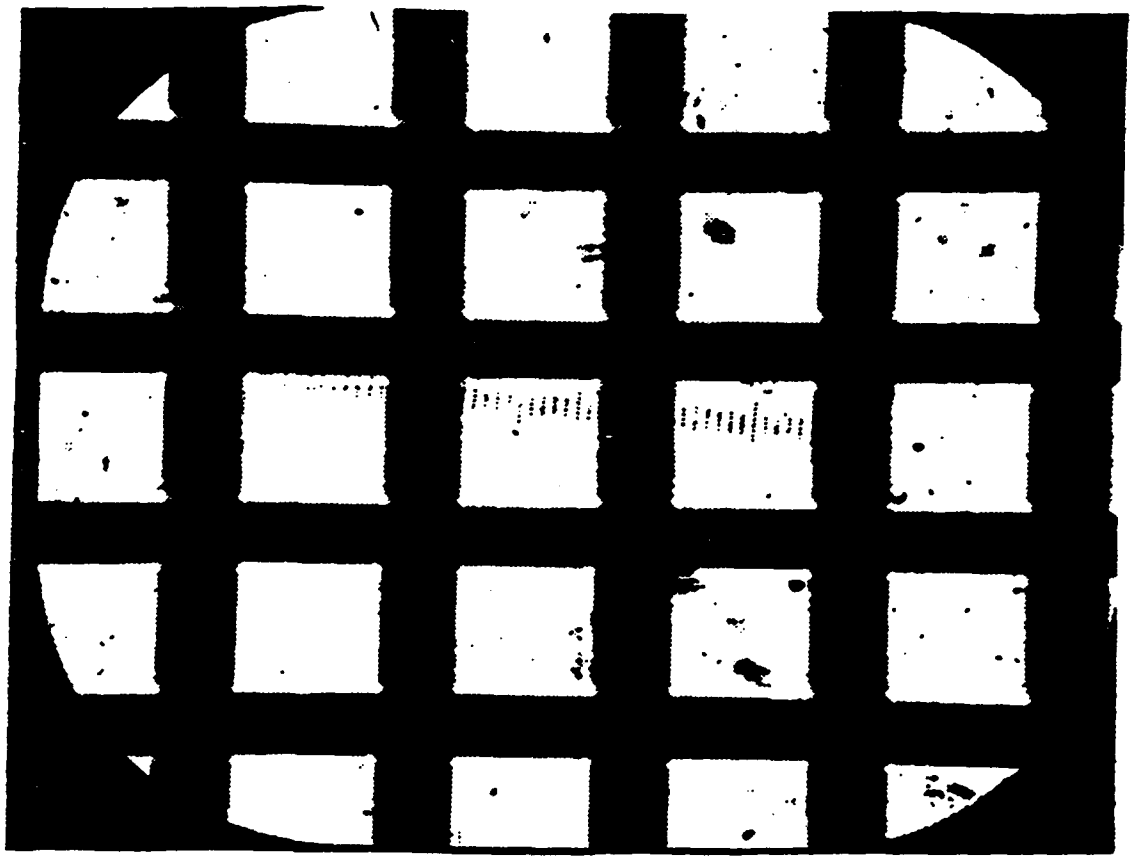

Figure 3.5. Photograph of the pixel structure of the Epson LCD.

does not fully characterize the Epson LCD and is presented here as a reference point for later discussions. A photograph of the image of a tank encoded in coherent light by the Epson LCD is shown in Figure 3.8. The transmission as a function of bias voltage was also measured for the Epson LCD in the same manner as that described for the Seiko LCTV. The plot of transmitted light versus bias voltage is shown in Figure 3.9.

D. Phase Modulation

The phase modulation property of the Epson LCDs has also been investigated in this research. The Mach-Zehnder interferometer shown in Figure 3.10 provided an excellent means for measuring the phase shift achievable using these televisions. The polarization of the light incident on the LCTV is aligned to be parallel with the molecular director on the

front surface of the device. The output analyzer is aligned perpendicular to the input polarization. A $\lambda/2$ plate is used to align the polarization of the reference beam with that of the object beam. The (0,0) order is then reimaged onto the Pulnix model 840 CCD camera to view the interference fringes.

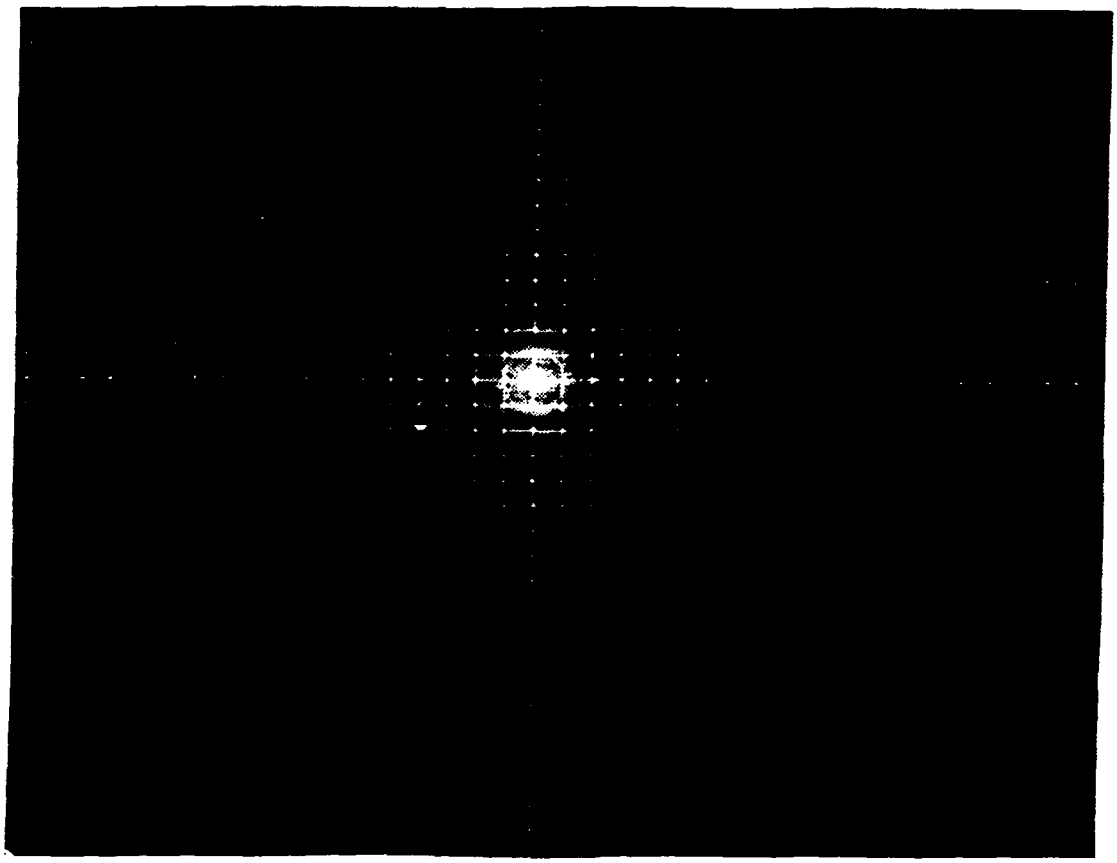

Figure 3.6. Photograph of the far field diffraction pattern due to the pixel structure.

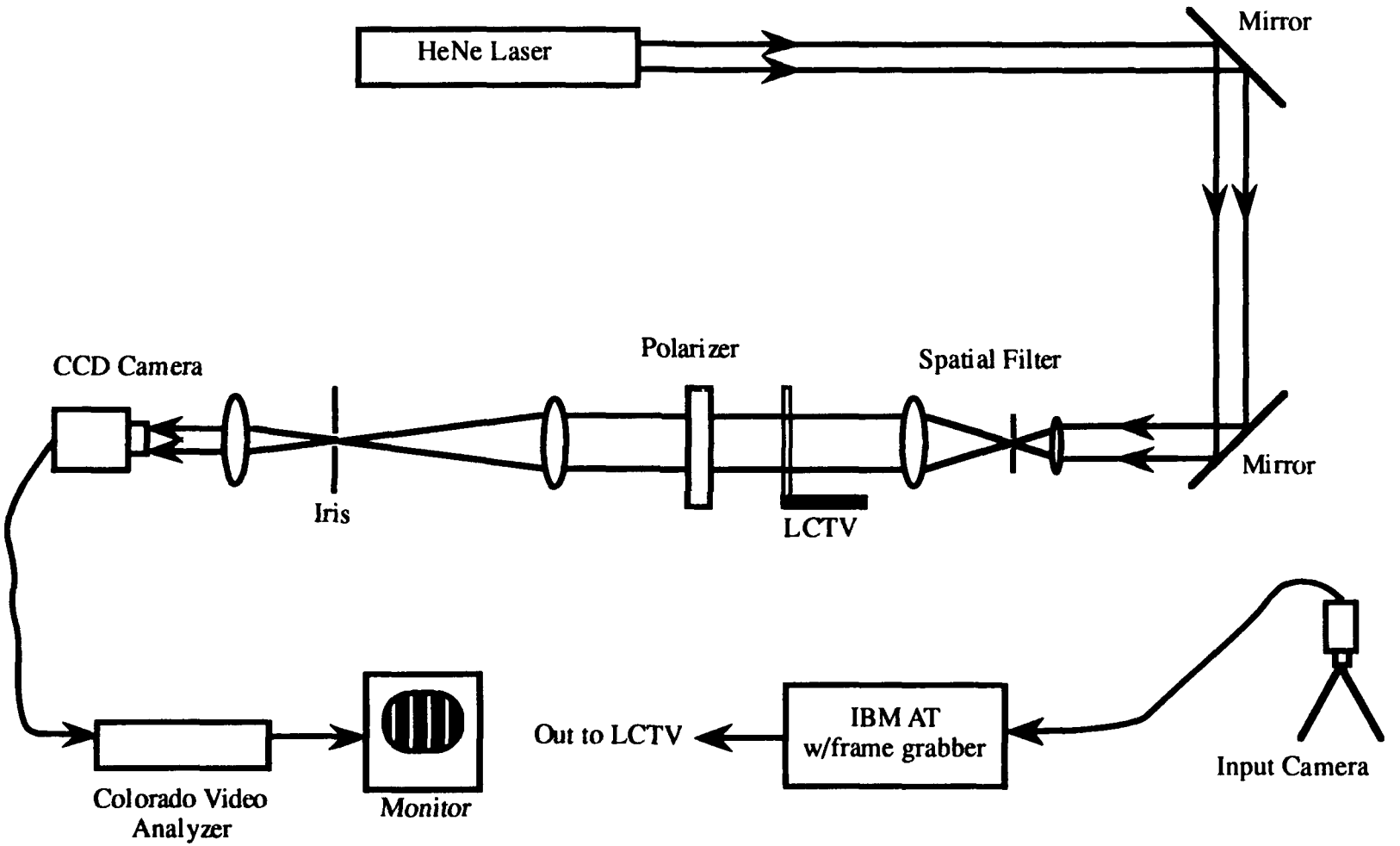

Figure 3.7. Optical system for measuring visibility.

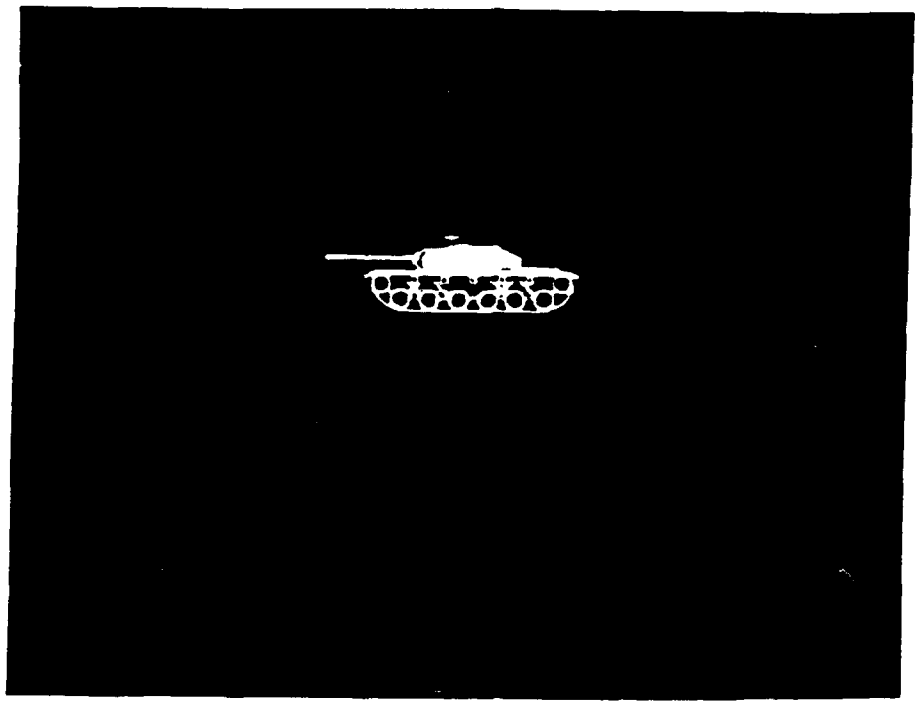

Figure 3.8. Photograph of the image encoded in coherent light by the Epson LCD.

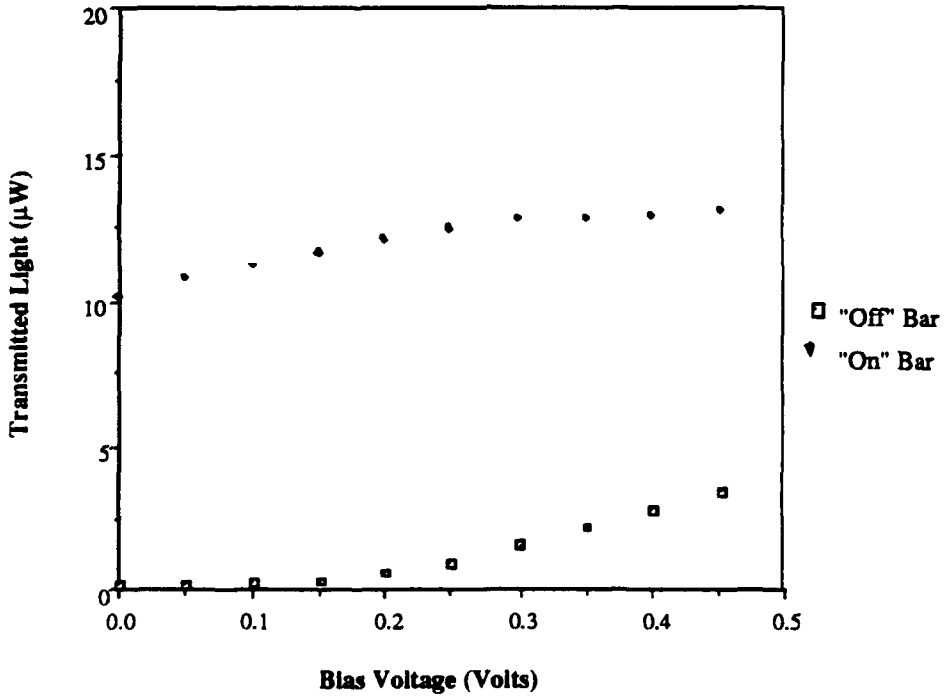

Figure 3.9. Transmitted light vs. bias voltage for the Epson LCD.

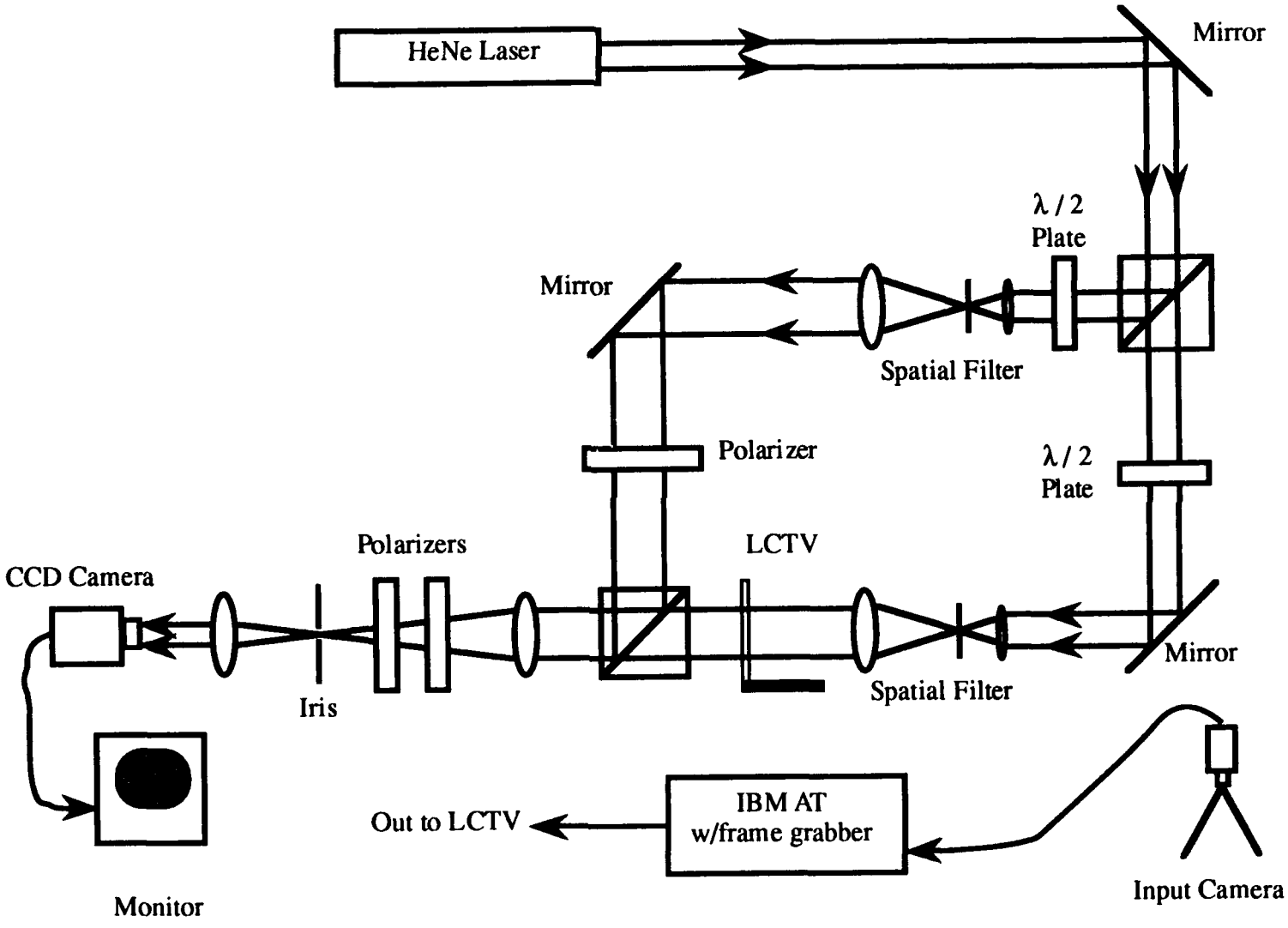

Figure 3.10. The Mach-Zehnder interferometer optical arrangement.

The same series of alternating bars used to measure the visibility is now used to measure the phase shift achieved between the "on" and "off" pixels. A photograph of the fringe structure will all pixels fully "off" is shown in Figure 3.11 while a photograph of the maximum fringe shift is shown in Figure 3.12. The phase shift was measured as a function of bias voltage. The bias voltage is a uniform DC offset applied to every pixel even in the "off state." This plot is shown in Figure 3.13. The maximum phase shift achieved between an "on" pixel and an "off" pixel was 1.87π or 336 degrees. A graph of the phase shift versus input video grey level was then constructed. This graph is shown in Figure 3.14.

E. Update Rate for the Epson LCTV

The addressing scheme for the typical LCTV has been discussed earlier in this report. The video information is transferred to the LCTV at field rates with the first and last eleven lines deleted. Each successive field overwrites the previous field contrary to the normal television interlaced field structure.

The update rate for the Epson LCTV was measured in the same manner as that for the Seiko LCTV using the system in Figure 3.15. Two cameras were used to view the spoke wheel pattern from slightly different angles. The cameras were such that the two images appeared side by side on the video output by the multiplexer. The multiplexer output was used as the input to the LCTV. The image encoded onto the laser light by the LCTV with the multiplexer switching at 60 Hz is shown in Figure 3.16. Again both patterns are visible and the update rate for the Epson LCTV has been verified to be 60 Hz.

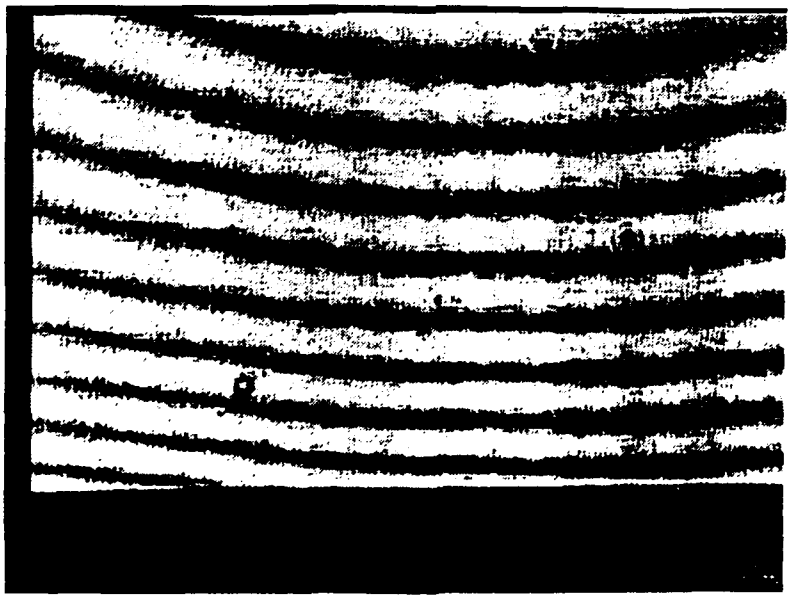

Figure 3.11. Photograph of the fringe structure with all pixels set to 0.

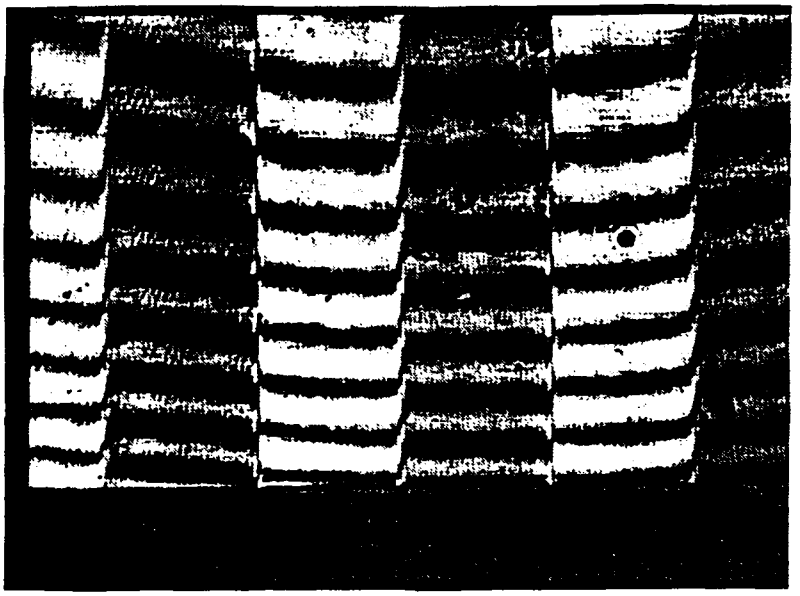

Figure 3.12. Photograph of the fringe structure with the bar pattern on the LCTV.

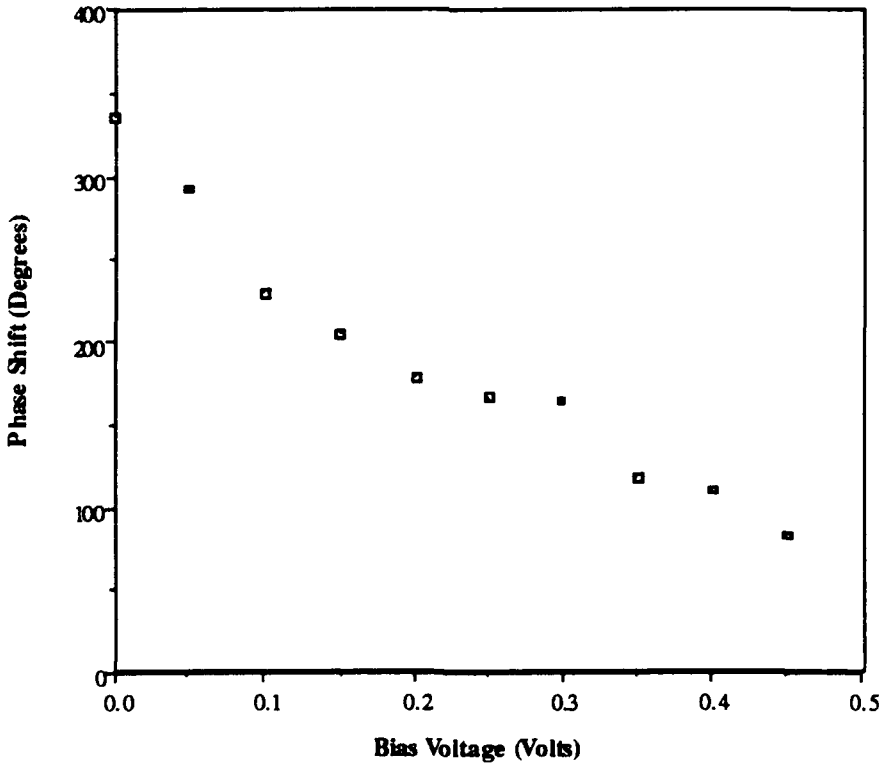

Figure 3.13 Phase shift vs. bias voltage for the Epson LCTV.

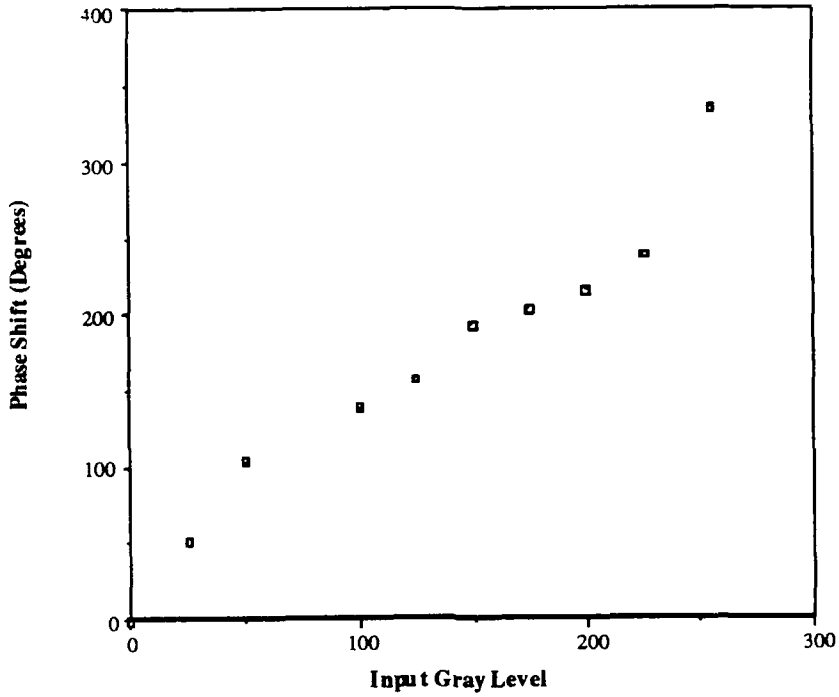

Figure 3.14. Phase shift vs. input gray level for the Epson LCTV.

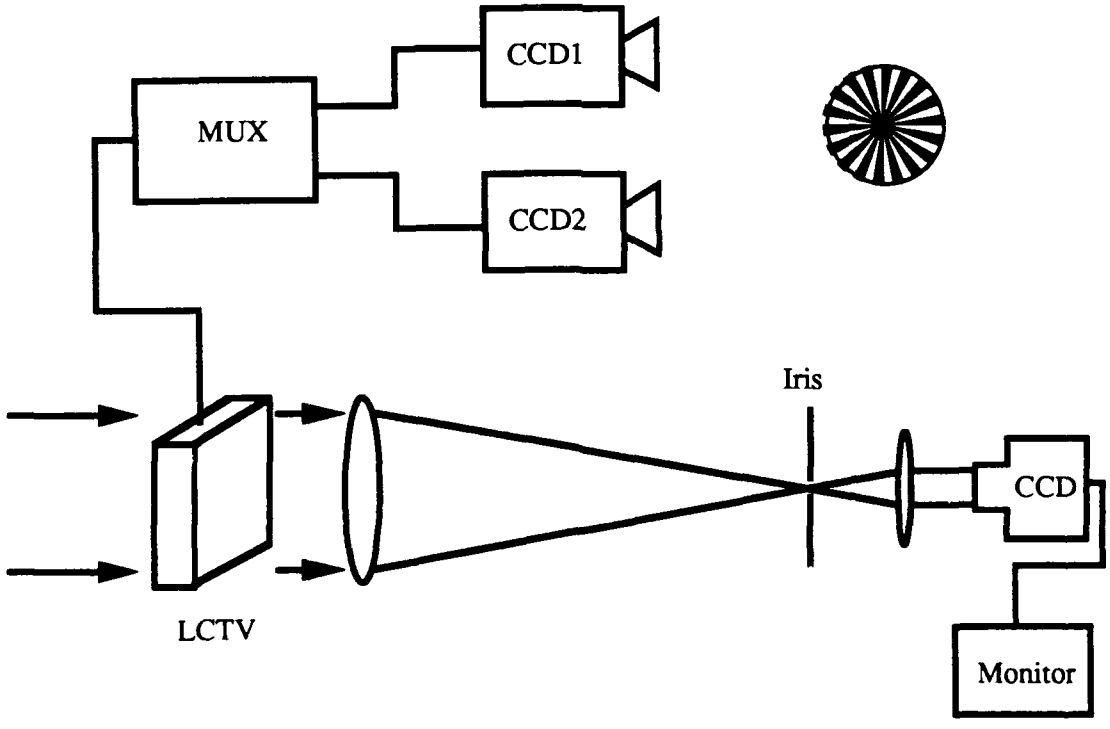

Figure 3.15. Architecture used to measure the LCTV update rate.

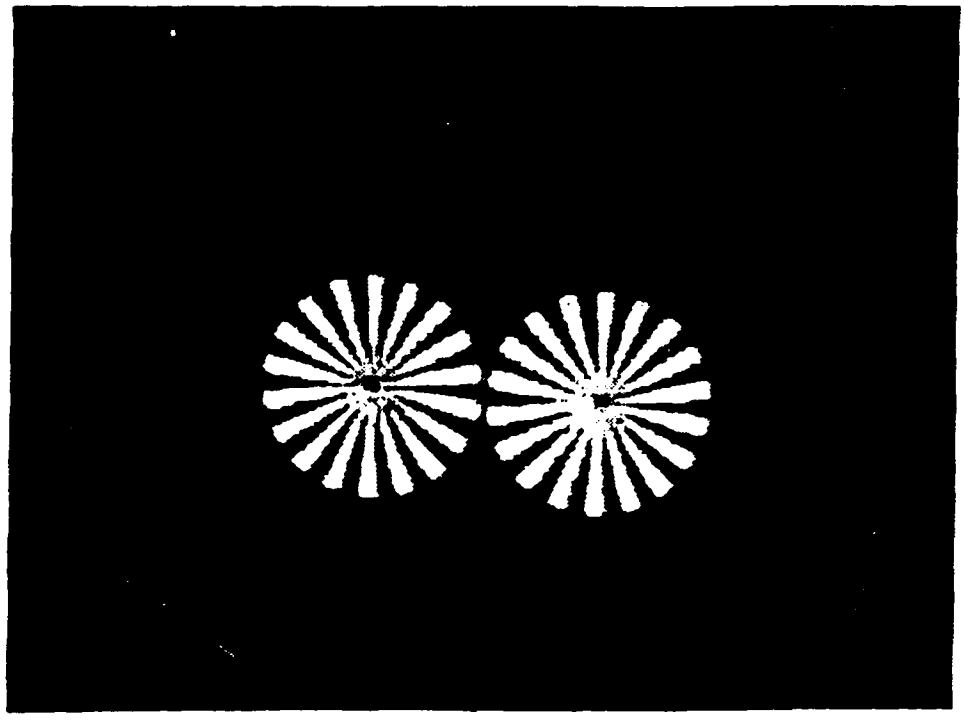

Figure 3.16. Photograph of the image encoded in coherent light by the Epson LCD with the multiplexer switching at field rates (60 Hz).

F. Polarization Rotation

The orientation of the molecular director for two of the LCTVs from the Epson projector was also determined. Linear polarized light which enters an LCTV parallel to the director will undergo a phase delay of:

$$\phi_e = \frac{2\pi n_e d}{\lambda} \qquad (3\text{-}3)$$

and emerge linearly polarized. Light which is polarized perpendicular to the director will undergo a phase delay of:

$$\phi_o = \frac{2\pi n_o d}{\lambda} \qquad (3\text{-}4)$$

but will still emerge linearly polarized. However, light which enters the LCTV polarized at some angle other than 0 or 90 degrees to the director will emerge elliptically polarized. The incident light can be decomposed into its components parallel and perpendicular to the

director. The two components will undergo different phase lags and this induces the elliptical exit polarization.

The polarization state of the exit light can be used to determine the orientation of the molecular director. Different orientations of linearly polarized light were passed through the LCTV and the output analyzer was rotated in an attempt to achieve a null for each orientation of incident light. Nulls can only be achieved with the analyzer for linearly polarized light. If a null is found, then, the input polarization must have been either parallel or perpendicular to the molecular director. For the light entering one side of the blue LCTV, nulls were found for incident light polarized at 96, 186, 276, and 6 degrees from the vertical. Nulls were also found for light entering from the other side of the LCTV. These nulls occurred for incident polarizations at 86, 176, 266, and 356 degrees from the vertical. Phase modulation was observed in the previous experiments with the input polarization oriented at 96 degrees to the vertical at one surface and at 176 degrees to the vertical at the other surface. No phase modulation was observed for the input polarization oriented at 186 degrees and 176 degrees to the vertical. Using the property of the LCTV which predicts phase modulation only for incident light polarized parallel to the molecular director, it was determined that the director is oriented at 96 degrees to the vertical at one surface and 176 degrees to the vertical at the other surface. The error in each of these polarization angle measurements is approximately ±3 degrees.

These measurements also indicate that the maximum twist in the molecules is only about 80 degrees rather than the desired 90 degrees. This is probably due to manufacturing defects in either forming the alignment layer or aligning the two glass plates which form the sandwich. The average polarization rotation between a fully "on" and fully "off" pixel is a function of the maximum twist in the molecules and the voltage which can be applied to the pixels. The maximum twist was measured with no power applied to the LCTV. The polarization rotation between "on" and "off" pixels must now be measured.

The orientation of the director was also determined for the red LCTV. Nulls were found at 111, 201, 291, and 21 degrees for light entering the LCTV from one side of the LCTV. Nulls were found at 11, 101, 191, and 281 degrees for light entering from the opposite face of the device. The phase modulation characteristics of this LCTV were again used to determine the correct orientation of the director. It was found that the director lies at 111 degrees from the vertical on the input side of the LCTV and is oriented at 191 degrees from the vertical at the output face. Again, the maximum twist in the director between the two faces is 80 degrees. The orientations of the directors for the two LCTVs are illustrated in Figure 3.17. Again, the error is about ±3 degrees.

The polarization rotation was also measured as described for the Seiko LCTV. A scene which consisted of a fully "off" bar (0 out of 255) on one-half of the screen and a fully "on" bar (255 out of 255) on the other side of the screen was displayed on the LCTV. The input polarization was aligned perpendicular to the molecular director to ensure no phase modulation occurred. The (0,0) order of the LCTV's Fourier transform was then reimaged onto a photodetector. The black (0) portion of the scene was blocked and the bias (or brightness) voltage was varied over its full range. The output analyzer was rotated to achieve the maximum reading on the photodetector for each bias voltage. The same

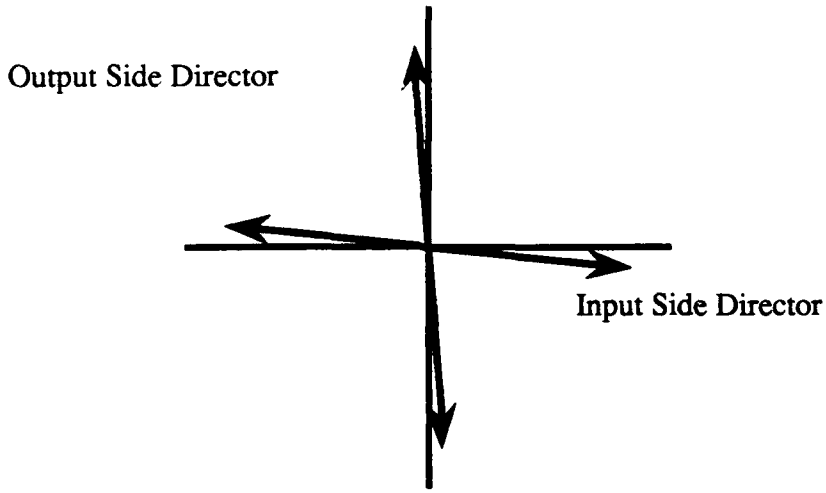

(a)

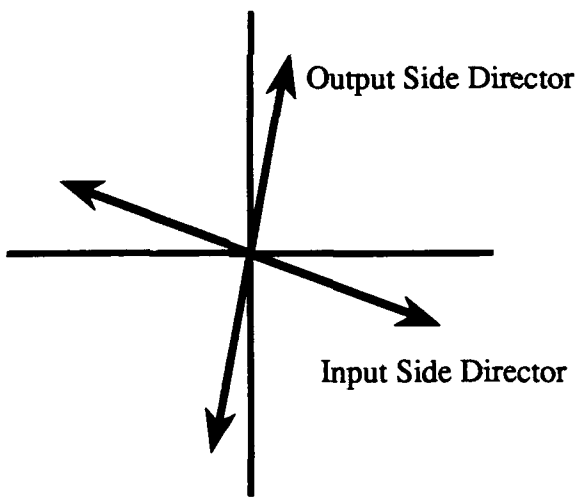

(b)

Figure 3.17. Orientation of the molecular director at the front and back surfaces for (a) the blue LCD and (b) the red LCD.

procedure was repeated with the white (255) portion of the bar blocked and only the black (0) bar incident on the detector. The two plots are shown in Figure 3.18. It is evident from the two curves that the maximum polarization rotation between a black and white pixel is 65 degrees.

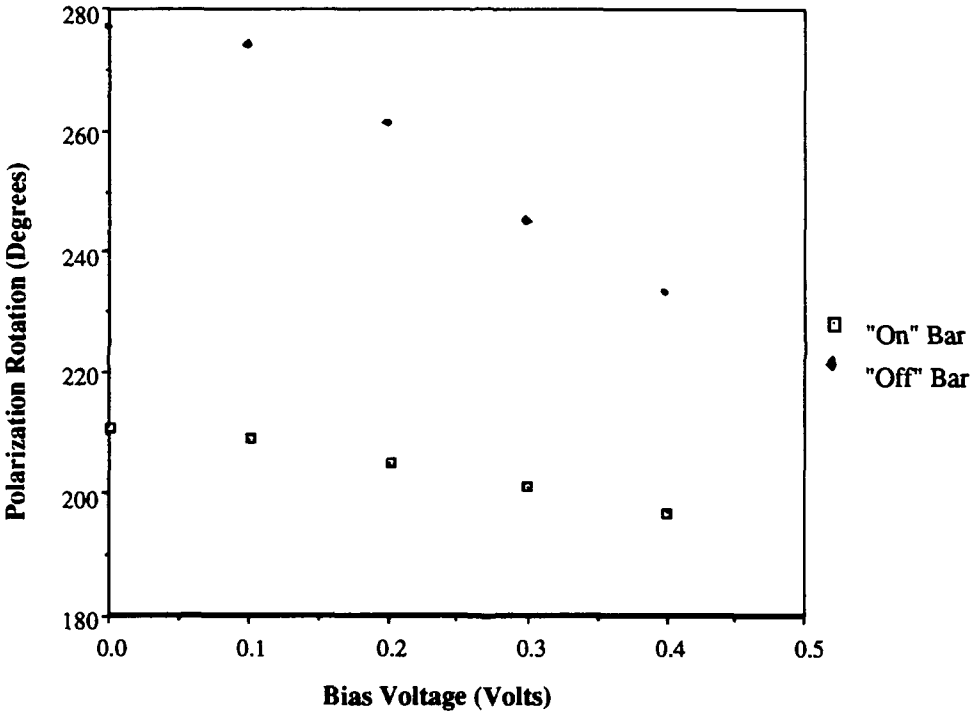

Figure 3.18. Polarization rotation vs. bias voltage for the Epson LCD.

IV. PHASE-MOSTLY JOINT TRANSFORM OPTICAL CORRELATOR

A. Background

Optical correlators have been around for many years. The first such architecture was the matched filtering optical correlator proposed by VanderLugt in 1963 [24]. The VanderLugt correlator, as it is commonly known, offers extremely high signal-to-noise ratios but suffers from alignment sensitivities of the matched filter in the frequency plane. This particular architecture will be discussed in more detail in a later chapter.

The Joint Transform Correlator (JTC) was first proposed by Weaver and Goodman as a method for optically convolving two images [25]. Rau presented the first experimental results at almost the same time [26]. The JTC architecture discussed in both papers is shown in Figure 4.1. The two input functions are illuminated with collimated coherent light and the Fourier transform formed by the lens. A photographic plate is used as a square-law detector to record the intensity spectrum in the Fourier plane. The photographic plate is then developed and placed in a collimated beam of coherent light. A converging lens is used to perform the Fourier transform of the intensity spectrum which yields the cross-correlation of the two input functions.

The JTC can be analyzed mathematically in the following manner. Consider two input functions $g(x,y)$ and $h(x,y)$ with Fourier transforms $G(\Omega_x,\Omega_y)$ and $H(\Omega_x,\Omega_y)$, respectively. These two functions are offset from the origin in the input plane by $+y_o$ and $-y_o$. The corresponding Fourier transforms can then be found by applying the Fourier shift theorem.

$$F\{g(x,y+y_o)\} = G(\Omega_x,\Omega_y)\exp(-j2\pi y_o\Omega_y) \tag{4-1}$$

$$F\{h(x,y-y_o)\} = H(\Omega_x,\Omega_y)\exp(+j2\pi y_o\Omega_y) \tag{4-2}$$

where $F\{\cdot\}$ denotes the Fourier transform operation. In the Fourier plane, the two transforms add coherently to form:

$$U = G\exp(-j2\pi y_o\Omega_y) + H\exp(+j2\pi y_o\Omega_y) \tag{4-3}$$

The joint transform power spectrum (JTPS) is recorded by the photographic plate and is given by:

$$I = UU^* = |G|^2 + |H|^2 + HG^*\exp(j4\pi y_o\Omega_y) + GH^*\exp(-j4\pi y_o\Omega_y) \tag{4-4}$$

The photographic plate is developed and placed in the collimated beam of light. The Fourier transform of the recorded JTPS is:

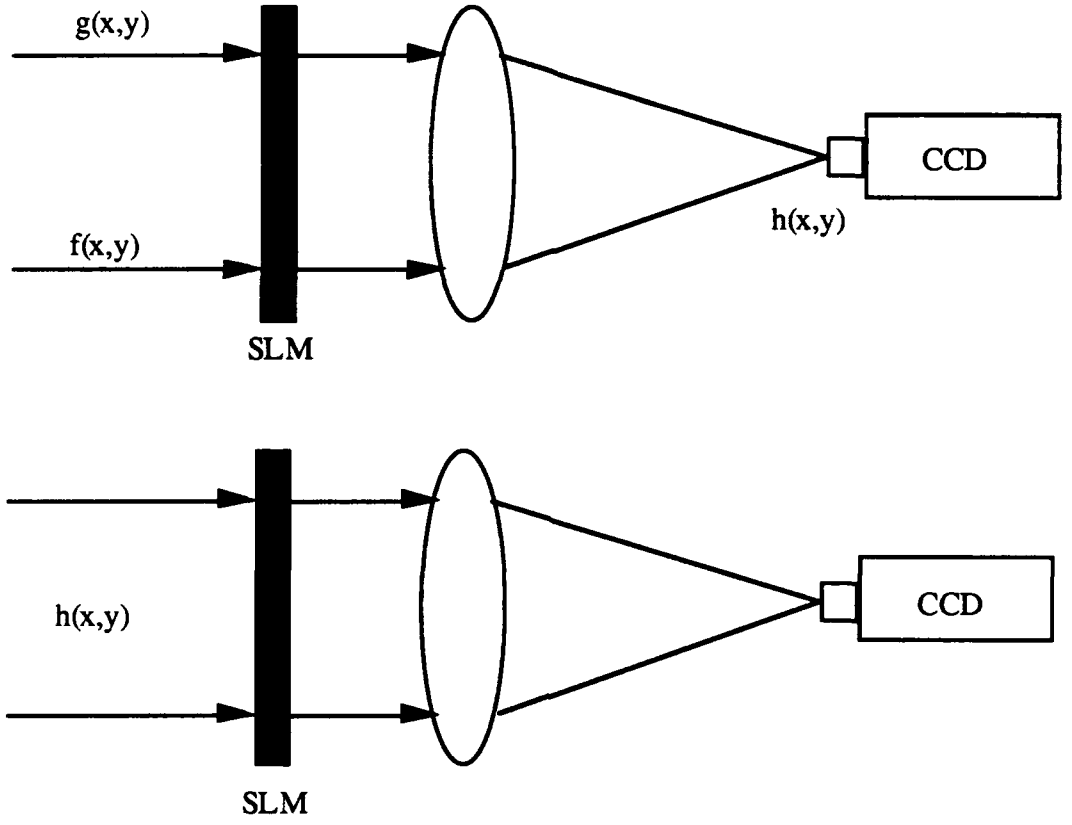

Figure 4.1 Optical architecture of a joint transform correlator.

$$F\{I\} = F\{GG^*\} + F\{HH^*\} + F\{HG^*\exp(j4\pi y_o\Omega_y)\} + F\{GH^*\exp(-j4\pi y_o\Omega_y)\} \quad (4\text{-}5)$$
$$= g^*g^* + h^*h^* + h^*g^{**}\delta(y-2y_o) + g^*h^{**}\delta(y+2y_o)$$

where * denotes the convolution operation. The first two terms of Equation 4-5 represent the autocorrelation of g and h, respectively. These two functions will be centered at the origin. The third term of Equation 4-5 is the crosscorrelation of h with g centered at $(0,y_o)$ while the fourth term is the cross-correlation of g with h centered at $(0,-y_o)$.

$$F\{I\} = g\bigstar g + h\bigstar h + h\bigstar g * \delta(y-2y_o) + g\bigstar h * \delta(y+2y_o) \quad (4\text{-}6)$$

The JTC can be used for pattern recognition applications by calling g or h the reference, or target, image. Recalling Equation 4-4 with g = h:

$$I = |G|^2 + |G|^2 + |G|^2 \exp\left(j4\pi y_o \Omega_y\right) + |G|^2 \exp\left(-j4\pi y_o \Omega_y\right) \tag{4-7}$$

$$I = 2|G|^2 + 2|G|^2 \cos\left(4\pi y_o \Omega_y\right) \tag{4-8}$$

Again transforming the JTPS yields:

$$F\{I\} = 2(g \bigstar g) + 2(g \bigstar g)\left[\delta(y-2y_o) + \delta(y+2y_o)\right] \tag{4-9}$$

The first term is again centered at the origin while the second term represents the two off-axis correlation signals centered at $\pm 2y_o$.

One disadvantage of the joint transform correlators discussed so far is the use of a photographic plate to record the JTPS. Rau first obviated the need for a photographic plate by replacing it with a vidicon camera [27]. The JTPS was then Fourier transformed using a spectrum analyzer. Casasent et al. demonstrated the first all-optical JTC [28]. A liquid crystal light valve served as the square-law detector to record the JTPS. The JTPS was then read out by a second collimated beam and Fourier transformed optically with a lens to yield the correlation signals.

Yu et al. presented the results obtained from an LCTV based JTC in 1986 (see Figure 4.2) [29]. A Seiko LVD202 color LCTV was used to present both the input scene and the reference image to the optical system. A lens performed the Fourier transform and the JTPS was detected with a CCD camera. A microscope objective was placed at the focal plane of the transform lens to magnify the fringe structure of the JTPS to accommodate the relatively low resolution of the camera. The JTPS was displayed on a second LCTV, Fourier transformed, and the resultant correlation signals detected by a second CCD camera. Again, a microscope objective was required to magnify the correlation plane such that the camera could resolve the correlation signals.

A novel innovation in the JTC architecture was introduced in 1989 when Gregory presented results from a time-multiplexed, single modulator JTC [30]. The two legs of the optical system shown in Figure 4.2 are identical. Gregory proposed and later demonstrated multiplexing of the input/reference scene with the resultant JTPS in successive frames (see Figure 4.3). The input modulator switched between the input/reference scene and the JTPS while the Fourier plane camera alternated between the JTPS and the correlation signals. A video demultiplexer was then used to separate the JTPS (for routing to the input modulator) and correlation signal (for display on a TV monitor) frames. Other authors have proposed methods for improving correlator efficiency and increasing the correlation signal-to-noise ratio by modifying the JTPS with some sort of nonlinearity [31] or by using multiple copies of the JTPS in the second leg of the JTC [32]. One problem with using the JTC outside the laboratory environment is its sensitivity to relative differences in the amplitudes of the input and reference scenes [33]. Recently, a method for building a JTC which is invariant to these relative differences has been proposed but not yet demonstrated [34].

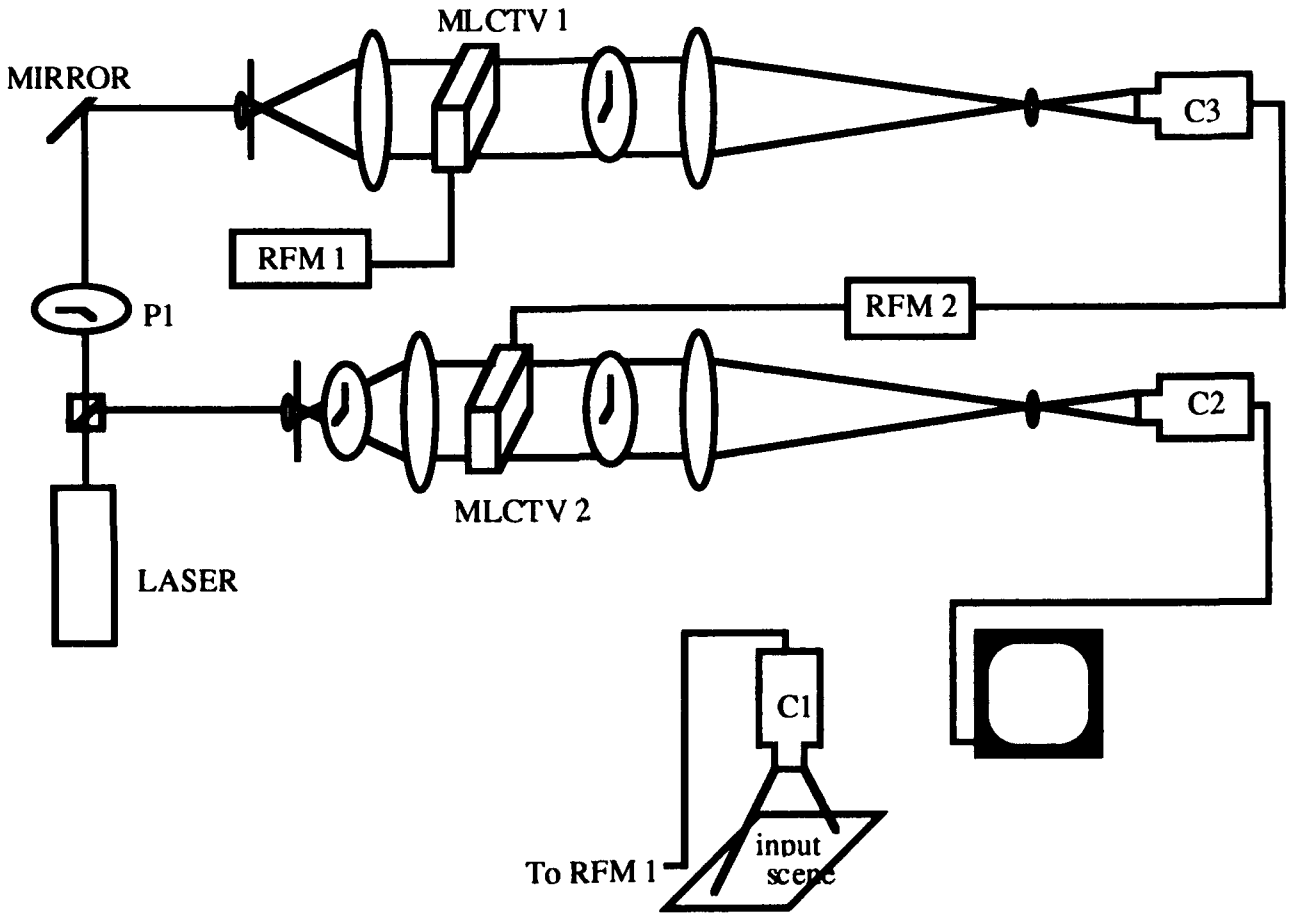

Figure 4.2. LCTV based joint transform optical correlator.

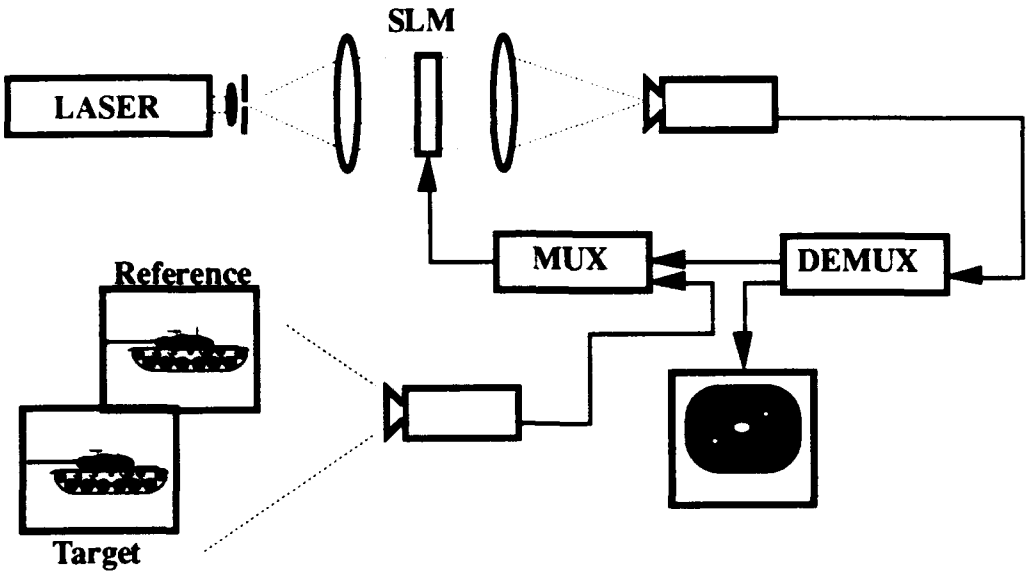

Figure 4.3 Single modulator joint transform correlator.

B. Phase-Mostly Joint Transform Correlator

The LCTVs in Figure 4.2 were operating in the traditional amplitude modulating mode discussed previously. It was found that the polarizers could be removed from the system and the LCTVs adjusted to operate in the phase-mostly mode as presented in Chapter 1. The JTC shown in Figure 4.4 was constructed using two Seiko LVD202 LCTVs operating in this phase-mostly mode. The low quality polarizers provided with the LCTV have been removed. The polarization of the beam illuminating the LCTVs was linear and aligned with the molecular director on the front of the televisions. No polarizers, except for the polarizing beamsplitter, were present in the system.

The input scene for this experiment is shown in Figure 4.5. The hoops were chosen for their easily identifiable Fourier transform. The brightness control on each LCTV was adjusted to provide the best possible fringe pattern and correlation signals. These are shown in Figures 4.6 and 4.7, respectively. The information encoded on the coherent light by each LCTV is mostly phase although some amplitude modulation is present. This amplitude modulation arises from a combination of a weak dichroism in the liquid crystal and polarization effects of the Fourier transform lenses.

The LCTVs were removed from the JTC and placed individually in the Mach-Zehnder interferometer arrangement discussed in Chapter 2. An alternating series of eight black and white bars was displayed on the LCTV and the fringe shift between "ON" and "OFF" pixels was measured. The phase shift in the input LCTV was found to be 128 degrees. The phase shift in the fringe LCTV was found to be 129 degrees. The visibility in the absence of an analyzer was also measured. The same bar pattern was displayed on the LCTV and a scan across the resulting image made using a Colorado Model 321 video

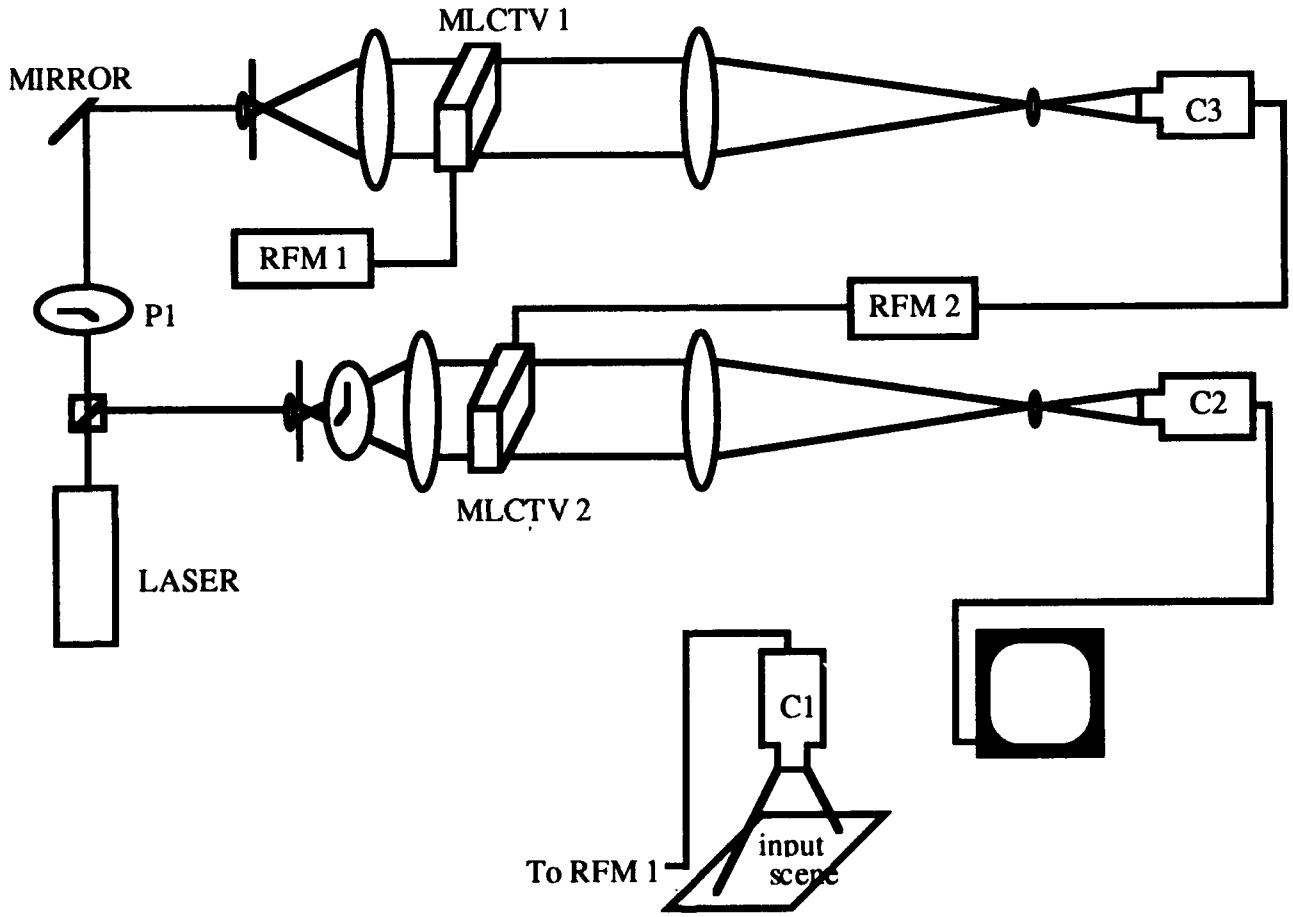

Figure 4.4. LCTV based phase mostly joint transform optical correlator.

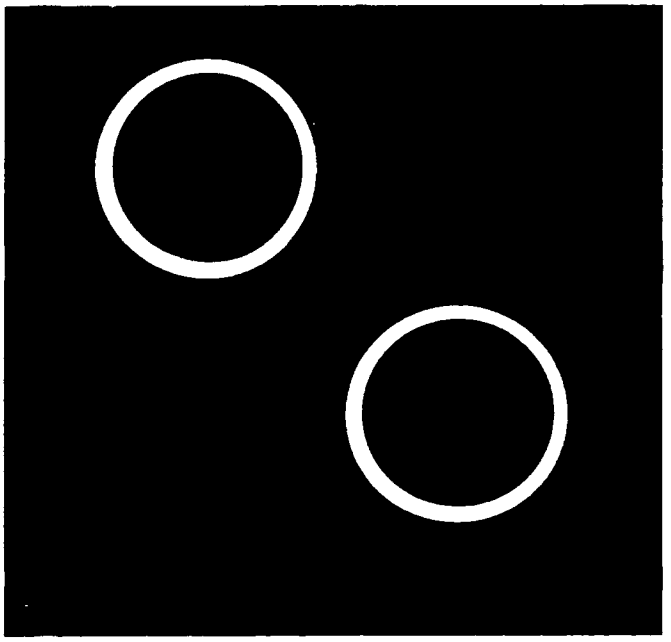

Figure 4.5. Input scene to phase-mostly joint transform correlator.

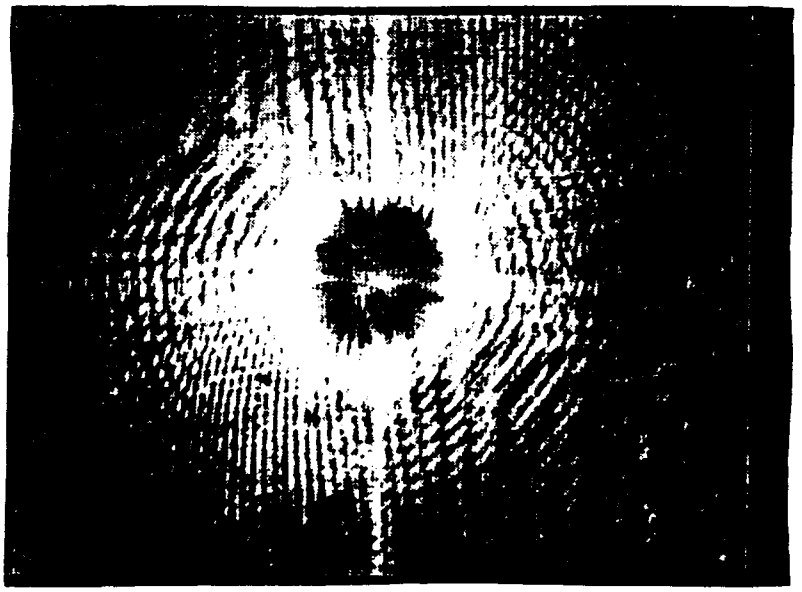

Figure 4.6. Photograph of fringes from hoop input to JTC.

analyzer and a Houston Instruments chart recorder in the same manner discussed in Chapter 2. The maximum visibility on both LCTVs was found to be 0.17. Photographs of the weak amplitude information encoded by the LCTVS are shown in Figure 4.8 and Figure 4.9.

The light utilization efficiency of this "phase mostly" operation was also measured. In this "phase mostly" mode, a transmission efficiency of 28% was measured for a single LCTV. The transmission efficiency was determined by measuring the intensity incident on the LCTV and the intensity transmitted by the LCTV. A transmission efficiency of only 5% was measured for a single LCTV operated in the amplitude mode. This transmission efficiency was determined by measuring the intensity prior to the LCTV and after the output analyzer. This technique assumes a linearly polarized laser output.

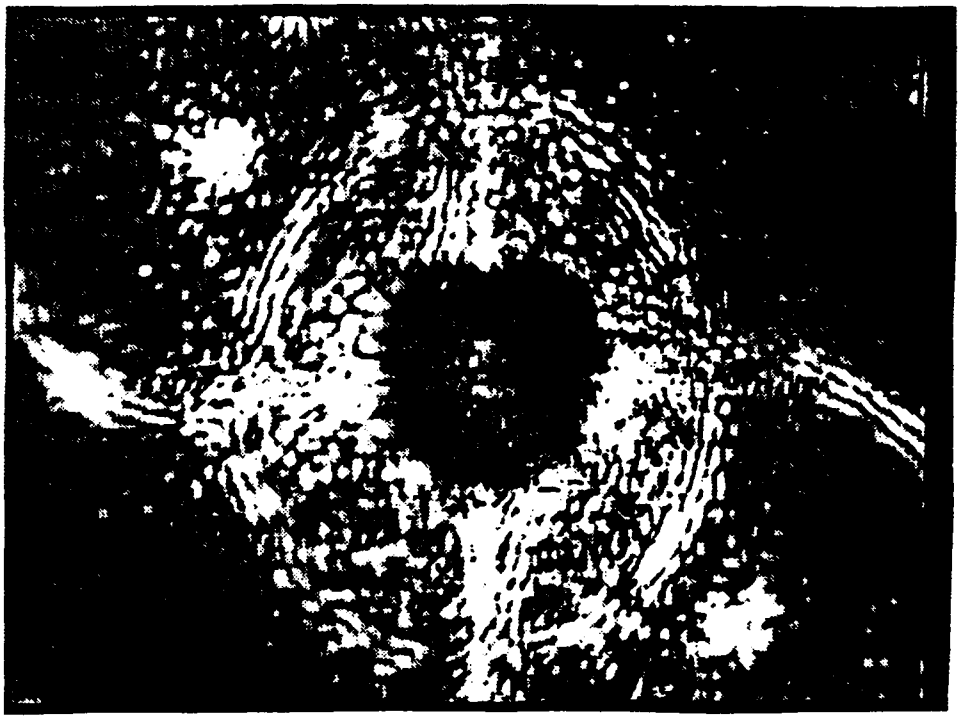

Figure 4.7. Photograph of saturated correlation signals from hoop input to JTC.

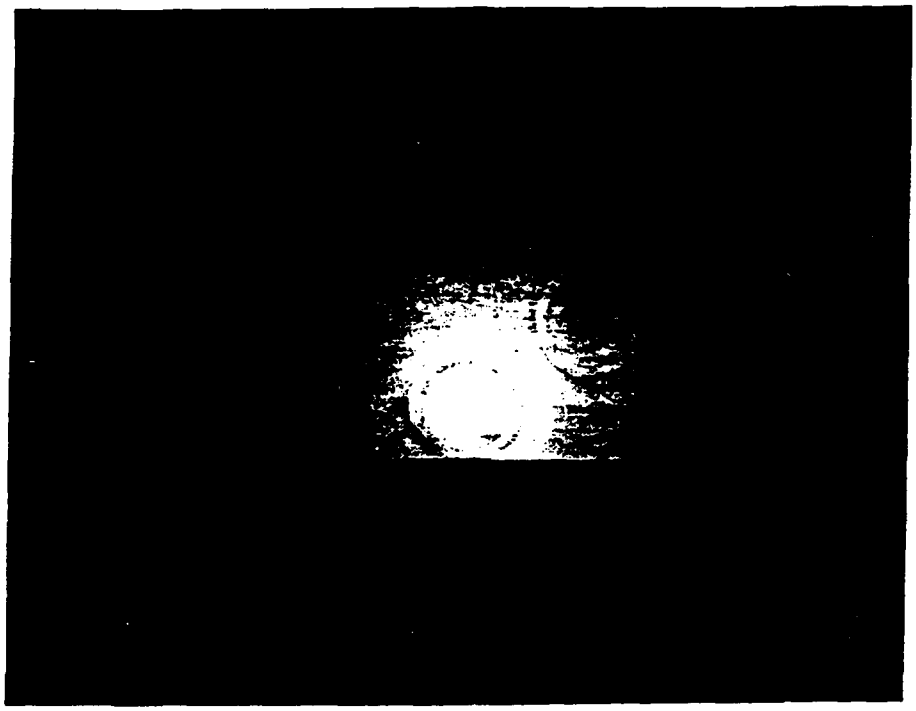

Figure 4.8. Photograph taken immediately after the input LCTV to illustrate the minimal amplitude information present.

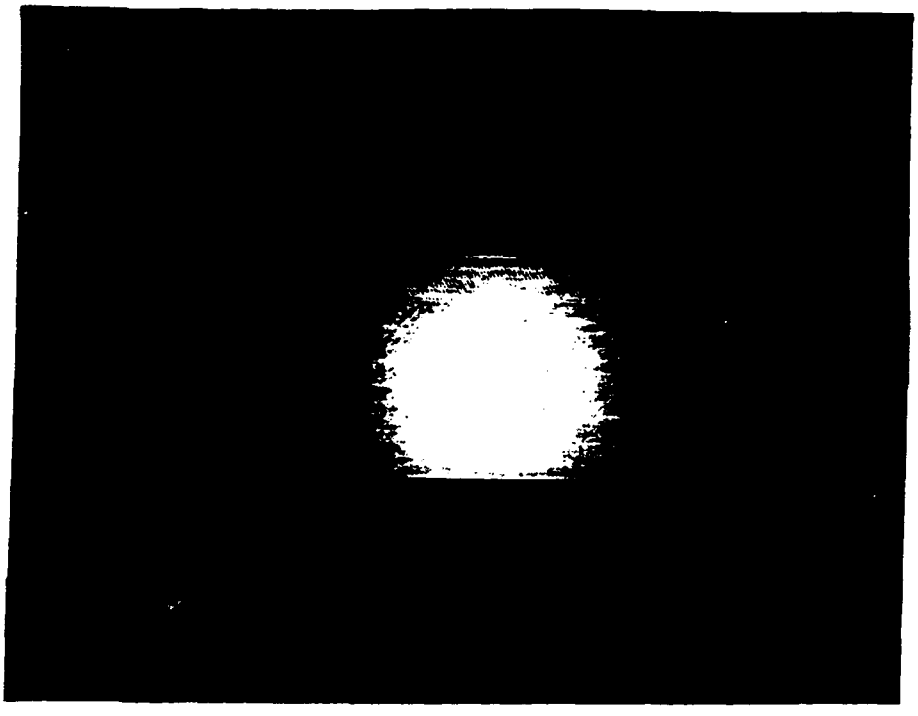

Figure 4.9. Photograph taken immediately after the fringe LCTV to illustrate the minimal amplitude information present.

V. THE VANDERLUGT OPTICAL CORRELATOR

A. Background

The VanderLugt correlator was first introduced in 1963 as a method for performing complex spatial filtering in a coherent optical system [35]. VanderLugt verified his theory by constructing a complex filter designed to detect the presence of an "L" in a scene of geometrical shapes. The cross-correlation present in the output plane demonstrated the capability of this system to detect and locate the target of interest.

The optical system arrangement of a VanderLugt correlator is shown in Figure 5.1. The off-axis reference beam at the focal plane can be represented by [36]:

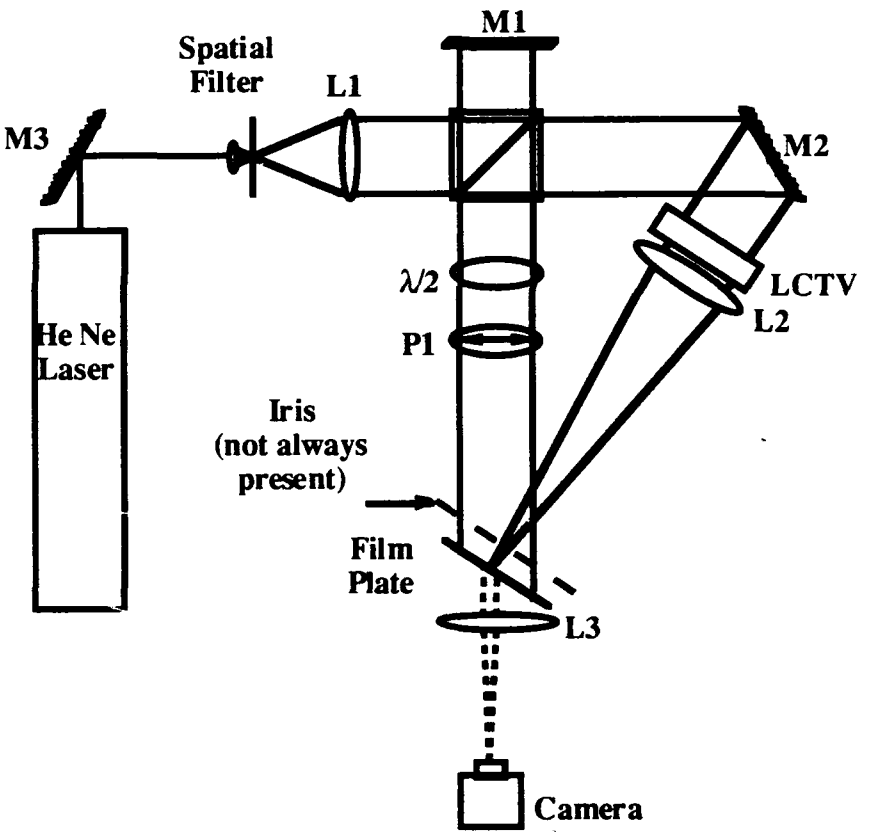

Figure 5.1. Architecture of the VanderLugt optical correlator.

$$U_r(x_f, y_f) = r_0 \exp(-j2\pi\alpha y_f) \tag{5-1}$$

where

$$\alpha = \frac{\sin(\theta)}{\lambda} \tag{5-2}$$

and θ is the reference beam angle. The input object has an amplitude transmittance given by h(x,y), whose Fourier transform is:

$$F\{h(x,y)\} = \frac{1}{\lambda f} H\left(\frac{x_f}{\lambda f}, \frac{y_f}{\lambda f}\right) \tag{5-3}$$

The object wave is Fourier transformed by the lens and interfered with the reference wave in the focal plane of the lens.

$$\begin{aligned} U_f\left(\frac{x_f}{lf}, \frac{y_f}{lf}\right) &= \frac{1}{\lambda f} H\left(\frac{x_f}{\lambda f}, \frac{y_f}{\lambda f}\right) + U_r(x_f, y_f) \\ &= r_0 \exp(-j2\pi\alpha y_f) + \frac{1}{\lambda f} H\left(\frac{x_f}{\lambda f}, \frac{y_f}{\lambda f}\right) \end{aligned} \tag{5-4}$$

The intensity of this interference is $U_f U_f^*$.

$$I_f \propto r_0^2 + \frac{r_0}{\lambda f} H^* \exp(-j2\pi\alpha y_f) + \frac{r_0}{\lambda f} H \exp(j2\pi\alpha y_f) + \frac{1}{(\lambda f)^2} HH^* \tag{5-5}$$

This intensity pattern is recorded on a piece of film. The developed film has a transmission which is proportional to the recorded intensity.

$$t \propto r_0^2 + \frac{r_0}{\lambda f} H^* \exp(-j2\pi\alpha y_f) + \frac{r_0}{\lambda f} H \exp(j2\pi\alpha y_f) + \frac{1}{(\lambda f)^2} HH^* \tag{5-6}$$

The input to this system (with the reference beam blocked) is g(x,y). The field transmitted by the VanderLugt filter is:

$$U_2 \propto \frac{1}{\lambda f} r_0^2 G + \frac{r_0}{(\lambda f)^2} GH^* \exp(-j2\pi\alpha y_f) + \frac{r_0}{(\lambda f)^2} GH \exp(j2\pi\alpha y_f) + \frac{1}{(\lambda f)^3} GHH^* \tag{5-7}$$

where G is the Fourier transform of g. The inverse transform is taken with the second lens. The field in the output plane of the correlator is given by:

$$U_3 \propto r_0^2 g + \frac{r_0}{(\lambda f)} g \bigstar h(x, y-\alpha\lambda f) + \frac{r_0}{(\lambda f)} g^* h(x, y+\alpha\lambda f) + \frac{1}{(\lambda f)^2} g^* h^* h(-x,-y) \qquad (5\text{-}8)$$

The first and last term of Equation 5-8 will form the DC component of the output plane. The second component is the off-axis cross correlation of the input scene with the reference filter. The third term is the convolution of the input scene with the reference scene and will be centered at $(0,-\alpha\lambda f)$.

B. Phase-Mostly VanderLugt Correlator

Much work has been done in the area of phase-only filtering in a VanderLugt correlator. Little work has been done using a phase modulating input device in the correlator although recently Horner and Sonef have presented some simulation results [37]. The Epson LCTV offers an excellent opportunity to expand the efforts in phase-only or phase-mostly inputs to the VanderLugt architecture.

The optical system in Figure 5.1 is the well-known VanderLugt matched filtering correlator. The input to this particular correlator was provided by the Epson LCTV operating in a "phase-mostly" mode. Note that the only polarizer in the system is located in the reference beam and serves only to match polarizations with the object beam. The $\lambda/2$ plate is used to adjust the relative intensity of the reference wave. A 762 mm focal length lens was used to perform the Optical Fourier Transform (OFT) in the object beam. The $\lambda/2$ plate following the laser was used to align the linear polarization of the object beam with the molecular director of the LCTV.

The optimum setting for the brightness control was determined by monitoring the OFT of a well-known input scene - a hoop. The hoop was displayed on the LCTV and optically Fourier transformed. A microscope objective was placed in the Fourier plane to magnify the information so that it could be monitored by the Pulnix Model 840 CCD camera. The transform was monitored as the brightness control was adjusted. The optimum brightness setting was defined as that which produced the most distinct OFT.

The matched filter for this case was recorded on a Kodak Type 131 holographic plate. The plate was exposed, developed, and replaced in the system. The iris just prior to the Fourier plane was used to block all but the center order of the LCTV transform and was present only when addressing the filter. The reference beam was blocked at this point and the correlation plane monitored with a Pulnix model 840 CCD camera. The target for this case was the tank in Figure 5.2.

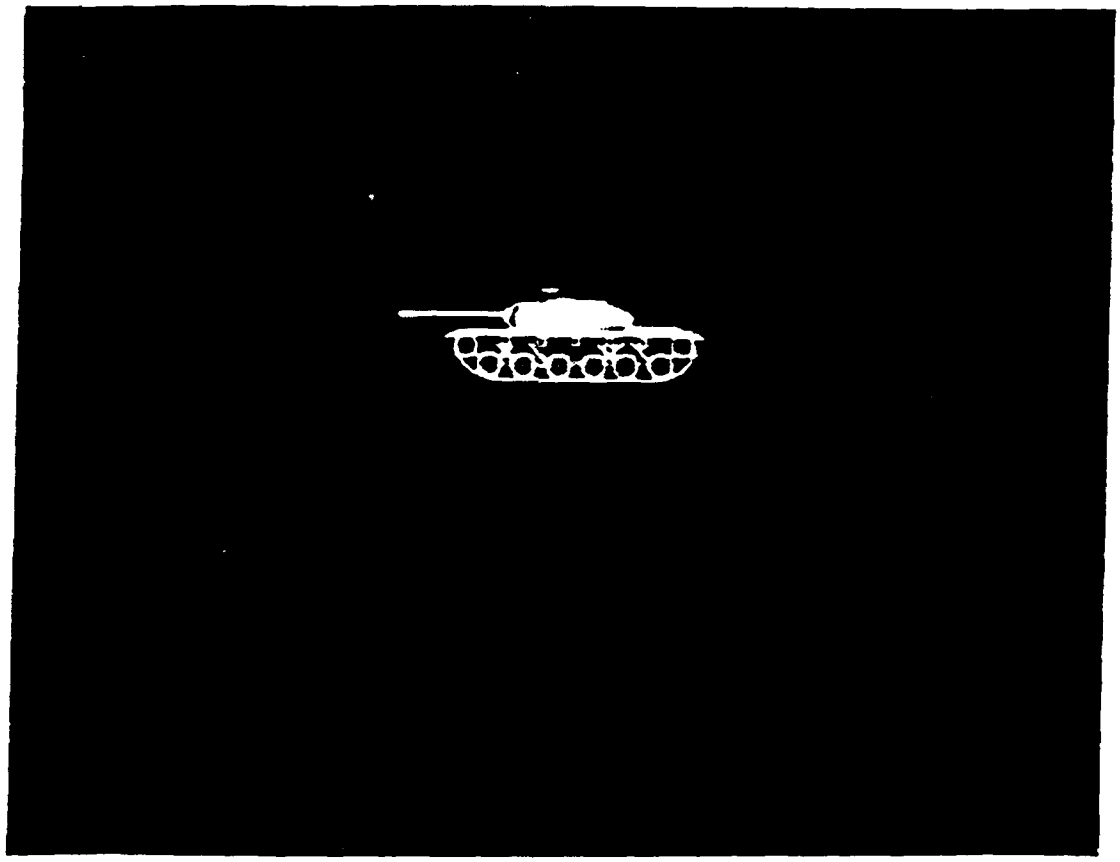

Figure 5.2. Input scene displayed on the LCTV.

The correlation plane is shown in Figure 5.3. The correlation peak is saturating the camera. The secondary peaks result from the reconstruction of the reference wave by the grating in the matched filter. A neutral density (ND) filter with a transmission of 6.4 percent was used to reduce the correlation peak intensity to a point below camera saturation. A scan was made along the x-axis through the secondary peaks and the correlation signal. The plot is shown in Figure 5.4. The correlation peak to first order peak ratio was 8 dB. A scan was also taken through the correlation signal along the y-axis (Figure 5.5). The noise was below the camera sensitivity so the ND filter was removed to record the noise level. The effects of the ND filter were taken into account in measuring the correlation peak and the correlation peak to average clutter ratio was found to be 28 dB.

C. Hybrid Modulation Effects

The LCTV was removed from the VanderLugt system and placed in the Mach-Zehnder interferometer discussed earlier. The phase shift was measured by displaying the 8 white and black bars on the TV and measuring the resultant fringe shift. The phase shift between fully "ON" and fully "OFF" pixels was found to be 235°.

The visibility of the image written in the coherent laser light without the analyzer was measured as discussed previously. Scans with the Colorado video analyzer were taken through the white and dark bars at several places and the average visibility (with no analyzer) was found to be 0. The difference between the intensity in the white and dark bars was indistinguishable from variations in intensity across the illuminating coherent light. A photograph of the bar pattern as displayed on the LCTV is shown in Figure 5.6. Only the change between the white and black bars is visible. This is probably caused by the weak dichroism present in the liquid crystal material or polarization effects due to the Fourier transform lens.

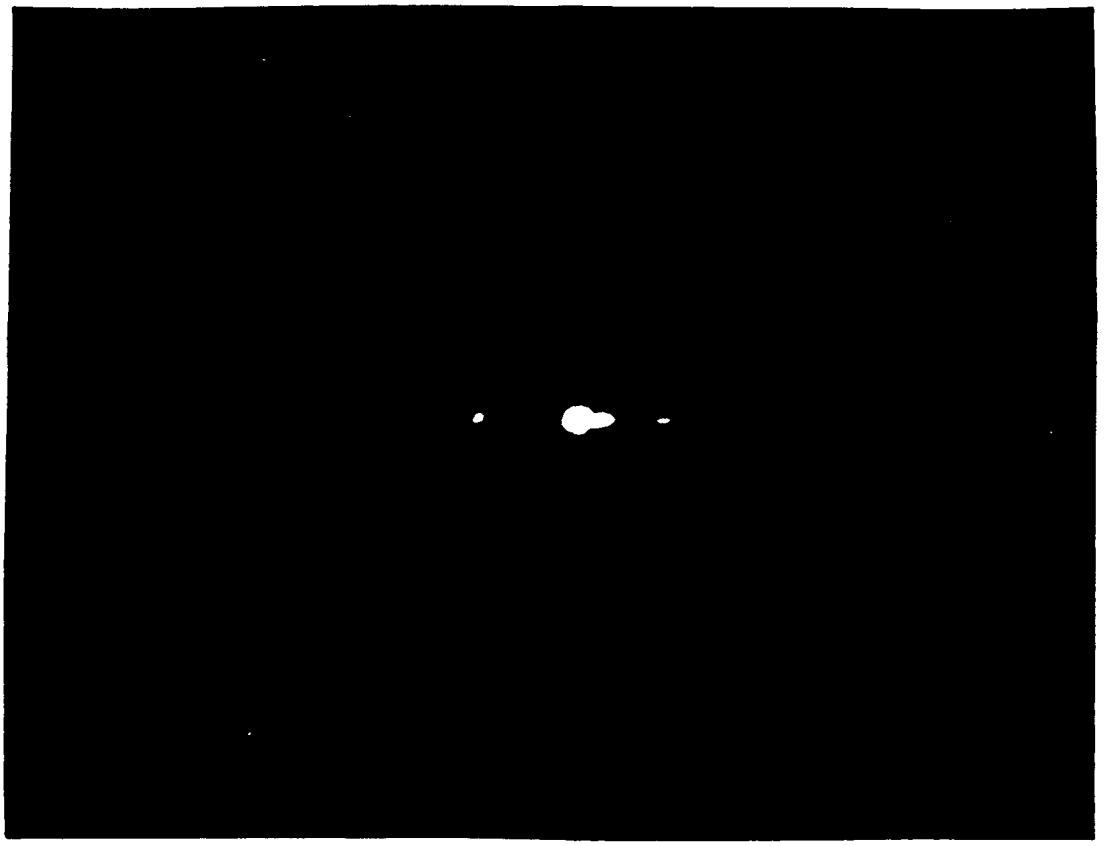

Figure 5.3. Correlation signal from phase-mostly VanderLugt correlator.

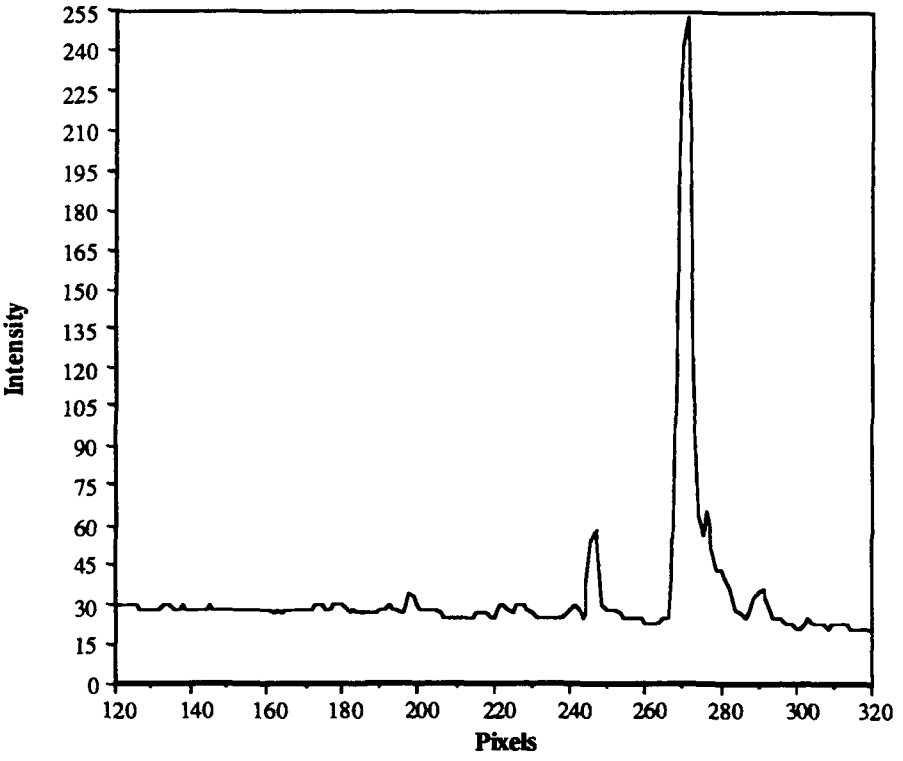

Figure 5.4. Scan through the correlation peak along the x-axis.

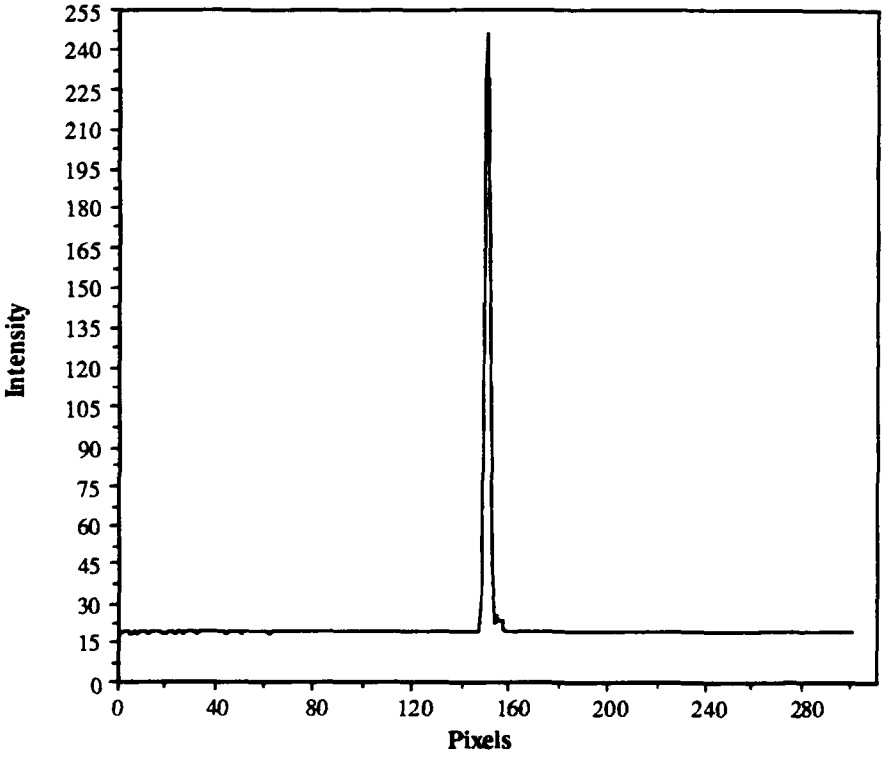

Figure 5.5. Scan through the correlation peak along the y-axis.

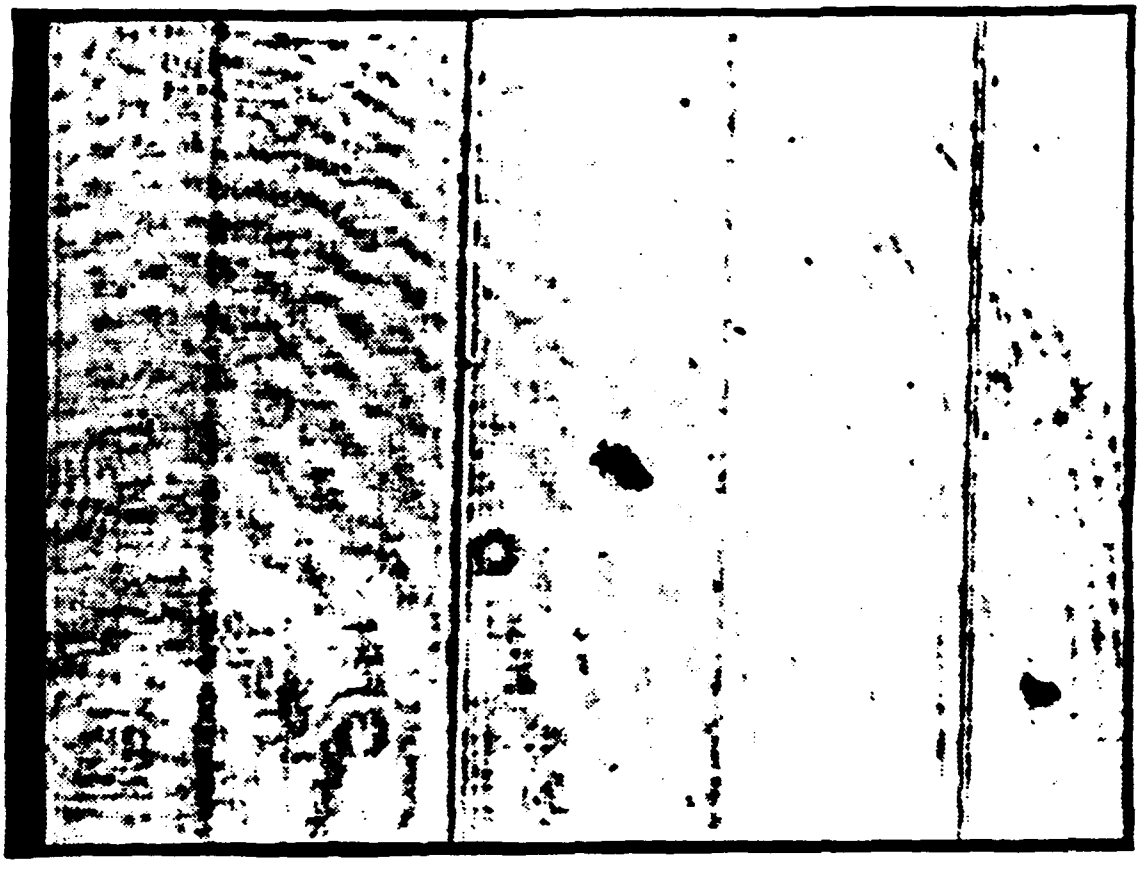

Figure 5.6. Photograph illustrating minimal amplitude information encoded by the LCTV.

VI. CONCLUSIONS AND DIRECTIONS FOR FUTURE RESEARCH

The intent of the research described in this report was to fully determine the modulation characteristics of two different LCTVs and to apply these properties in two different optical correlator architectures. The Seiko LCTV was found to have a visibility of 0.94 (C = 33:1). This TV was also capable of modulating 340 degrees of phase between an "on" pixel and an "off" pixel. The Epson LCTV achieved an average visibility of 0.96 (C = 49:1) in an amplitude modulation configuration and one TV was found to modulate more than 330 degrees of phase.

The Seiko LCTV served as both an input and filter plane modulator in a joint transform correlator. The need for analyzers in the system was obviated by using the phase modulating characteristics to encode the information in the coherent laser light. The net result was a correlator with an increased light efficiency (28% per modulator instead of 5%) and better performance. The increased light efficiency meant more detectable fringes in the joint transform plane which, in turn, meant brighter correlation signals.

Similar results were obtained when using an Epson LCTV as a phase encoding input plane modulator in a VanderLugt correlator. The increased transmission efficiency resulted in a number of visible higher diffraction orders in the correlation plane. It should be noted that while a photographic filter was used in this research, some researchers have since built correlators using an Epson LCTV as a filter plane modulator. This work has yet to be published, however, it is known that the LCTV was used to display only a 128 x 128 binary phase filter. The research presented in this report will soon be extended to use the analog phase modulation characteristics of LCTVs to encode an analog phase filter.

Little attention has been given to using phase-encoded inputs in these correlators. Recently, a liquid crystal television was used as a phase encoding input device in a VanderLugt correlator and the results of this experiment were presented in Chapter 5 of this report. Some questions still remain, however. It has been suggested that changes in the depth of the phase modulation due to changes in the input scene illumination will significantly affect the output of the correlator.

While much attention has been paid in recent years to the development of phase only filters for use in VanderLugt correlators, the research presented here represents some of the first work in phase-only inputs to these correlators. This work, however, has prompted a few questions. It must be understood that a phase-only input, as discussed here, is really a phase-encoding of the intensity in the input scene. A change in input scene intensity will result in a change in the amplitude of the phase-encoding. This change in the input amplitude will change the phase in the Fourier transform plane. It is necessary, then, to show that these changes will not drastically affect the correlation signal or that phase-encoded inputs will only work in constant amplitude situations. Some preliminary simulations indicate that while the transform phase does change, the correlation signal peak is still quite good if the change is not too great. Future experiments will seek to quantify the amount of change in input amplitude that can be tolerated and to compare these results to an amplitude input case.

Liquid Crystal Televisions (LCTVs) have been exploited for both their amplitude and phase modulating properties independently. Future work will complete the picture by describing and building a full complex modulator using a pair of LCTVs. There are at least two architectures for accomplishing this task. The first is shown in Figure 6.1 [38]. The beamsplitter that produces the two addressing beams is not shown. Ultimately the LCTVs could be bonded to the beamsplitter itself. Careful examination of this architecture shows that the resulting image is:

$$m(x,y) = Af(x,y) + \exp[jBg(x,y)] \qquad (6\text{-}1)$$

where m(x,y) is a complex image formed by the coherent addition of purely phase and purely amplitude images. Any desired complex function could be achieved with the correct choice of f(x,y) and g(x,y). The coefficients A and B are device specific parameters.

A much simpler method to achieve the desired complex image is shown in Figure 6.2. The first LCTV is arranged between two flat sheet polarizers to achieve the amplitude modulation while allowing the LCTVs to be placed in close proximity to one another. It is assumed that the LCTVs will be close enough to avoid diffraction effects between the two

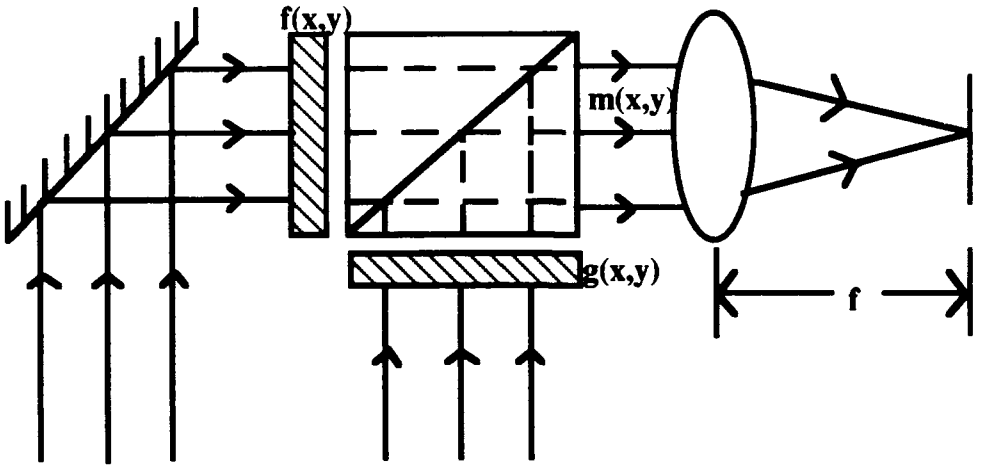

Figure 6.1. Architecture for coherently adding phase and amplitude information encoded by two LCTVs.

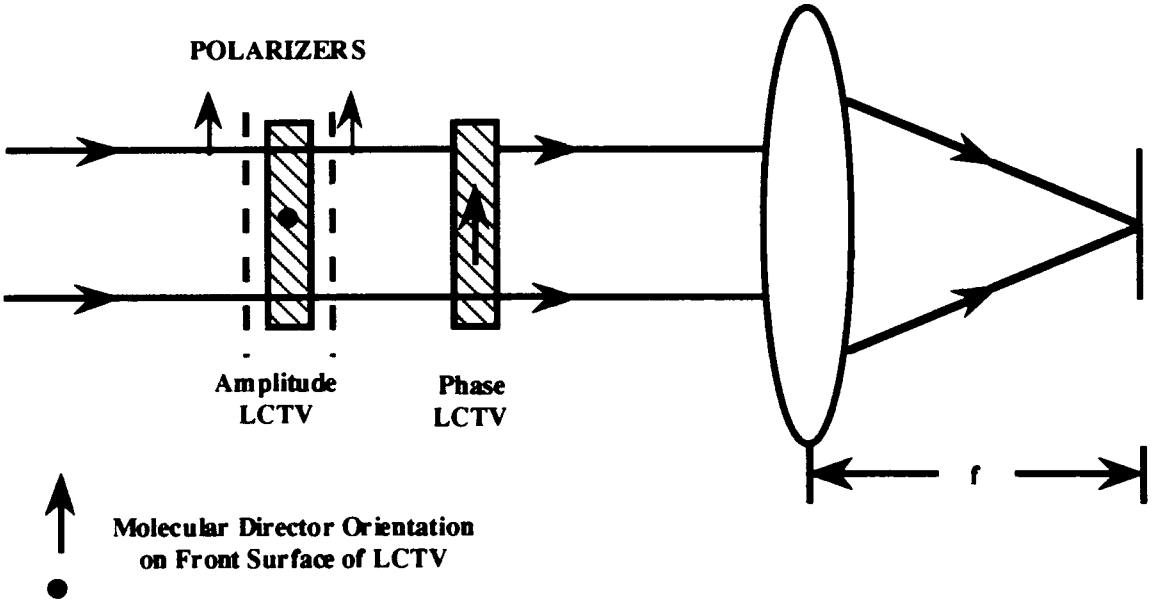

Figure 6.2. Architecture for coherently multiplying the phase and amplitude information encoded by two LCTVs.

devices. If this is not the case, the first LCTV can be imaged 1:1 onto the second LCTV to avoid this problem. The second LCTV modulates phase and the two images are combined in a multiplicative operation given by:

$$k(x,y) = Af(x,y)\exp[jBg(x,y)] \qquad (6\text{-}2)$$

This architecture has two distinct advantages over the system shown in Figure 6.1. The alignment is much easier to perform in a common path architecture and the choice of f(x,y) and g(x,y) is much easier to make. All of the phase information is contained in the second modulator (displaying g(x,y)) and all of the amplitude information in contained in the first modulator (displaying f(x,y)). This is not true for the system described by Equation 6-1. The phase term g(x,y) contributes both to the amplitude and the phase of m(x,y) and in like manner the amplitude term f(x,y) contributes to both components.

The architecture presented in Figure 6.2 lends itself to immediate application in optical filtering. This architecture will provide a fully programmable, updatable, full complex filter for use in any optical system. Optical correlation filters can now extend beyond binary phase-only to the multi-level phase - multi-level amplitude filter. More than two LCTVs can be cascaded, if necessary, to achieve the desired phase and amplitude encoding.

One concern of this approach is that the amplitude modulating LCTV will modulate some phase and the phase modulating LCTV will modulate some amplitude. This in fact does occur, but the effect is small. When the LCTV is in the phase modulating mode, an amplitude modulation of less than 5 percent can be observed with no output analyzer. Undesired phase modulation can be avoided by aligning the polarization of the input light perpendicular to the molecular director of the amplitude encoding LCTV. A complete analysis and evaluation of a full complex modulator based on two LCTVs would make an excellent research topic in itself.

This report has described in some detail the modulation characteristics of the Seiko and Epson LCTVs. These modulation characteristics have been applied to optical systems and the results are very encouraging. While much has been done with these devices, much work remains. Two promising avenues of research have been proposed and many more exist. Perhaps LCTVs will prove to be the modulator which allows optical computing to move from the laboratory into the real world.

REFERENCES

1. James C. Kirsch, Don A. Gregory, T. Dean Hudson, Jeffrey A. Loudin, and W. Michael Crowe, "Optical correlator field demonstration," in *Acquisition, Tracking, and Pointing V*, Michael K. Masten and Larry A. Stockum, eds., Proc. Soc. Photo-Opt. Instrum. Eng. 1482, 69-78, 1991.

2. Jason N. Duffey, T. Dean Hudson, and James C. Kirsch, "Optical evaluation of the microchannel spatial light modulator," in *Wave Propagation and Scattering in Varied Media II*, V. K. Varadan, ed., Proc. Soc. Photo-Opt. Instrum. Eng. 1558, 1991 (in publication).

3. James C. Kirsch and Don A. Gregory, "Video rate optical correlation using a magneto-optic spatial light modulator," Opt. Eng. **29**, 1122-1128 (1990).

4. Don A. Gregory, Richard D. Juday, Jeffrey Sampsell, Richard Gale, Robert W. Cohn, and Stanley E. Monroe, Jr., "Optical characteristics of a deformable-mirror spatial light modulator," Opt. Lett. **13**, 10-12 (1988).

5. Tracy D. Hudson, Don A. Gregory, and Robert K. Worcester, "Performance characteristics of an optically-addressed ferroelectric liquid crystal spatial light modulator," Appl. Opt., accepted 1991.

6. T. Dean Hudson, James C. Kirsch, and Don A. Gregory, "Comparison of optically addressed spatial light modulators," in *Optical Technology for Signal Processing Systems*, M. P. Bendett, ed., Proc. Soc. Photo-Opt. Instrum. Eng. 1474, 101-111, 1991.

7. E. Kaneko, *Liquid Crystal TV Displays: Principles and Applications of Liquid Crystal Displays* (D. Reidel Publishing Co, Boston, 1987), p. 15.

8. Ref. 7, p. 16.

9. K. Benson, *Television Engineering Handbook* (McGraw-Hill, New York, 1986), pp 13.16-13.17.

10. H. K. Liu, Jeffrey A. Davis, and R. A. Lilly, "Optical data processing properties of a liquid crystal television spatial light modulator," Opt. Lett. **10**, 635-637 (1985).

11. Matt Young, "Low-cost LCD video display for optical processing," Appl. Opt. **25**, 1024-1026 (1986).

12. Glenn D. Boreman and Edward R. Raudenbush, "Modulation depth characteristics of a liquid crystal television spatial light modulator," Appl. Opt. **27**, 2940-2943 (1988).

13. Ref. 7, p. 212.

14. Ref. 7, p. 17.

15. N. Konforti, E. Marom, and S. Wu, "Phase-only modulation with twisted nematic liquid crystal spatial light modulator," Opt. Lett. **13**, 251-253 (1988).

16. W. Bleha, L. Lipton, E. Wiener-Arnear, J. Grinberg, P. Reif, D. Casasent, H. Brown, and B. Markevitch, Opt. Eng. **17**, 371 (1978).

17. T. H. Barnes, T. Eiju, K. Matsuda, and N. Ooyama, "Phase-only modulation using a twisted nematic liquid crystal television," Appl. Opt. **28**, 4845-4852 (1989).

18. Francis T. S. Yu, Suganda Jutamulia, Tsongneng W. Lin, and Don A. Gregory, "Adaptive real-time pattern recognition using a liquid crystal TV based joint transform correlator," Appl. Opt. **26**, 1370-1372 (1987).

19. Don A. Gregory, Jeffrey A. Loudin, James C. Kirsch, Eddy C. Tam, and Francis T. S. Yu, "Using the hybrid modulating properties of the liquid crystal television," Appl. Opt. **30**, 1374- (1991).

20. E. Hecht and A. Zajac, *Optics* (Addison-Wesley, Reading, 1974), pp 290-292.

21. Eddy C. Tam, *Modulation properties of a twisted nematic liquid crystal spatial light modulator and its applications in a joint transform correlator*, Ph.D. dissertation, Pennsylvania State University, 30 (1990).

22. Ref. 21, p. 31.

23. Don A. Gregory, "Real-time pattern recognition using a modified liquid crystal television in a coherent optical correlator," Appl. Opt. **25**, 467-469 (1986).

24. Anthony VanderLugt, IEEE Transactions on Information Theory **IT-10**, 139-145 (1964).

25. C. S. Weaver and J. W. Goodman, "A technique for optically convolving two functions," Appl. Opt. **5**, 1248 (1966).

26. James E. Rau, "Detection of differences in real distributions," Journal of the Opt. Soc. of Am. **56**, 1490-1494 (1966).

27. James E. Rau, "Real-time complex spatial modulation," Journal of the Opt. Soc. of Am. **57**, 798-802 (1967).

28. David Casasent and Alan Furman, "Equalizing and coherence measure correlators," Appl. Opt. **17**, 3418-3423 (1978).

29. Francis T. S. Yu, Suganda Jutamulia, Tsongneng W. Lin, and Don A. Gregory, "Adaptive real-time pattern recognition using a liquid crystal TV based joint transfrom correlator," Appl. Opt. **26**, 1370-1372 (1987).

30. Jeffrey A. Loudin, Adam C. Hill, Jason N. Duffey, W. Michael Crowe, and Don A. Gregory, "Video multiplexing/demultiplexing single spatial light modulator optical correlator," Opt. Eng. **29**, 1129-1135 (1990).

31. B. Javidi, "Nonlinear joint power spectrum based optical correlation," Appl. Opt. **28**, 2358-2367 (1989).

32. Francis T. S. Yu, Eddy C. Tam, and Don A. Gregory, "High-efficiency joint-transform correlator," Opt. Ltr. **15**, 1029-1031 (1990).

33. Don A. Gregory, Jeffrey A. Loudin, and Francis T. S. Yu, "Illumination dependence of the joint transform correlation," Appl. Opt. **28**, 3288-3290 (1989).

34. Suganda Jutamulia, George M. Storti, Don A. Gregory, and James C. Kirsch, "Illumination-independent high-efficiency joint transform correlator," Appl. Opt. **30**, 4173-4175 (1991).

35. Anthony VanderLugt, IEEE Transactions on Information Theory **IT-10**, 139-145 (1964).

36. Joseph W. Goodman, *Introduction to Fourier Optics* (McGraw-Hill, San Francisco, 1968), p. 172.

37. Joseph L. Horner and R. A. Sonef, "Phase-dominant spatial light modulators," Electronics Letters **24**, 626-627 (1988).

38. James M. Florence and Richard D. Juday, "Full complex spatial filtering with a phase-mostly DMD," in *Wave Propagation and Scattering in Varied Media II*, V. K. Varadan, ed., Proc. Soc. Photo-Opt. Instrum. Eng. 1558, 1991 (in publication).

39. Ref. 36, pp.9-14.

LIST OF SYMBOLS

AOD	acousto-optic device
C	contrast ratio
CCD	charge-coupled device
d	thickness of liquid crystal
dB	decibel
dia	diameter
DEMUX	demultiplexer
DMD	deformable mirror device
EOD	electro-optic device
f	focal length of a lens
FELC	ferro-electric liquid crystal
HeNe	helium neon
Hz	Hertz
I_{min}	minimum light intensity
I_{max}	maximum light intensity
JTC	joint transform correlator
JTPS	joint transform power spectrum
λ	wavelength
$\lambda/2$	one-half wavelength
$\lambda/4$	one-quarter wavelength
LCD	liquid crystal display
LCLV	liquid crystal light valve
LCTV	liquid crystal television
lp/mm	line pairs per millimeter
L1, L2, L3	lenses
M1, M2, M3	mirrors
μm	micrometer
μW	microwatt
MLCTV	modified liquid crystal television
mm	millimeter
MOD	magneto-optic device
msec	millisecond
MSLM	microchannel spatial light modulator
MTF	modulation transfer function
MUX	multiplexer
ND	neutral density
n_e	extraordinary index of refraction
n_o	ordinary index of refraction
nm	nanometer
NRC	Newport Research Corporation
NTSC	National Television Systems Committee
OFT	optical Fourier transform
V	visibility

LIST OF SYMBOLS (cont'd)

ϕ_e	phase delay experienced by extraordinary wave
ϕ_o	phase delay experienced by ordinary wave
π	Pi
P1	polarizer
RFM	radio frequency modulator
sec	second
SLM	spatial light modulator
SNR	signal to noise ratio
θ	angle (theta)
TN-TE	twisted nematic - field effect
TFT	thin film transistor
TV	television

APPENDIX

APPENDIX. DERIVATION OF THE FOURIER TRANSFORM OF THE EPSON LCTV

One characteristic common to all pixelated SLMs is the structure of the far field diffraction pattern. The array of orders which results from the two dimensional array of apertures can, in some ways, be considered a drawback for electrically addressed modulators since most optical systems will only use one of the diffraction orders and the rest of the light is lost. The pixel structure can be modeled as a rectangular aperture convolved with a two dimensional comb function as follows:

$$t(x,y) = \left[\text{comb}\left(\frac{x}{a}\right)\text{comb}\left(\frac{y}{b}\right) * \text{rect}\left(\frac{x}{c}\right)\text{rect}\left(\frac{y}{d}\right)\right] \bullet \text{rect}\left(\frac{x}{e}\right)\text{rect}\left(\frac{y}{f}\right) \qquad \text{(A-1)}$$

where a, b, c, d, e, and f are the x and y dimensions of the array spacing, the pixel aperture, and the overall LCTV aperture, respectively. The far field diffraction pattern can be approximated by the Fourier transform of Equation A-1:

$$T(\Omega_x, \Omega_y) = F\{t(x,y)\} \qquad \text{(A-2)}$$

The spatial frequencies Ω_x and Ω_y are given by:

$$\Omega_x = \frac{x_f}{\lambda f} \text{ and } \Omega_y = \frac{y_f}{\lambda f} \qquad \text{(A-3)}$$

where x_f and y_f are the coordinates in the far field. Equation A-2 can be evaluated using well known Fourier transform theorems [39].

$$F\left\{\text{comb}\left(\frac{x}{x_0}\right)\right\} = x_0\text{comb}\left(x_0\Omega_f\right) \qquad \text{(A-4)}$$

$$F\left\{\text{rect}\left(\frac{x}{x_0}\right)\right\} = x_0\text{sinc}\left(x_0\Omega_f\right) \qquad \text{(A-5)}$$

$$F\{g * h\} = GH \qquad \text{(A-6)}$$

and

$$F\{g \cdot h\} = G * H \qquad \text{(A-7)}$$

where G and H are the Fourier transforms of g and h, respectively. The far field diffraction pattern is then:

$$T(x_f, y_f) = abcdef\left[\text{comb}(a\Omega_x)\,\text{comb}(b\Omega_y) \cdot \text{sinc}(c\Omega_x)\,\text{sinc}(d\Omega_y)\right] * \text{sinc}(e\Omega_x)\,\text{sinc}(f\Omega_y) \qquad \text{(A-8)}$$

The diffraction pattern described by Equation A-8 is exactly that shown in Figure 3.6 - a two dimensional sinc function due to the overall LCTV aperture convolved with an array of delta functions and the whole pattern is modulated by another two dimensional sinc function due to the pixels themselves. If an image, g(x,y), is displayed on the LCTV, the transmission function becomes:

$$t_1(x,y) = g(x,y) \bullet t(x,y) \qquad \text{(A-9)}$$

The far field diffraction pattern will be:

$$T_1(\Omega_x, \Omega_y) = G(\Omega_x, \Omega_y) * T(\Omega_x, \Omega_y) \qquad \text{(A-10)}$$

Equation A-10 describes an important property of the far field diffraction of pixelated SLMs - each order in the pattern will contain the Fourier transform of the input image g(x,y). For this reason, only one order is needed to perform any optical processing algorithms. While this means a drastic reduction in light efficiency, it also means that multiple copies of the Fourier transform of the image are available.

DISTRIBUTION

	Copies
Director U.S. Army Research Office ATTN: SLCRO-PH P. O. Box 12211 Research Triangle Park, NC 27709-2211	1
Headquarters Department of the Army ATTN: DAMA-ARR Washington, DC 20310-0623	1
Headquarters OUSDR&E ATTN: Ted Berlincourt The Pentagon Washington, DC 20310-0623	1
ITT Research Institute ATTN: GACIAC 10 W. 35th Street Chicago, IL 60616	1
U. S. Army Materiel System Analysis Activity ATTN: AMXSY-MP (Herbert Cohen) Aberdeen Proving Ground, MD 21005	1
Department of Electrical Engineering Pennsylvania State University ATTN: Dr. F. T. S. Yu University Park, PA 16802	1
Department of Physics The University of North Carolina at Charlotte ATTN: Dr. Eddy C. Tam Charlotte, NC 28223	1
Department of the Air Force Rome Labs ATTN: ESOP/Dr. Joe Horner Hanscom AFB, MA 01731–5000	1

	Copies
Dean, College of Science University of Alabama in Huntsville Materials Science Bldg, Room C207 Huntsville, AL 35899	1
Dr. James D. Brasher Teledyne Brown Engineering Optical Systems Department, Mail Stop 19 Cummings Research Park Huntsville, AL 35807–7007	1
Dr. William H. Carter Naval Research Laboratory, Code 8304 Washington, DC 20375	1
Dr. W. T. Cathey 228 Alpine Way Boulder, CO 80304	1
Dr. Arthur Chiou Rockwell International, MS A25A P.O. Box 1085 Thousand Oaks, CA 91358	1
Dr. John D. Downie NASA Ames Research Center Intelligent Systems Technology Branch, MS 244–4 Moffett Field, CA 94035	1
Dr. Marvin D. Drake The Mitre Corporation, MS E050 Burlington Road Bedford, MA 01730	1
Dr. F. Trevor Gamble Denison University Department of Physics Granville, OH 43023	1

	Copies
Mr. Joseph L. Horner 38 Oakley Road Belmont, MA 02178	1
Dr. Bahram Javidi University of Connecticut Electrical Engineering Department 260 Glennbrook Road, U–157 Storrs, CT 06269–3157	1
Dr. Sing H. Lee University of California, San Diego 9500 Gilman Drive, ECE Dept. La Jolla, CA 92093–0407	1
Dr. Freddie Liu Physical Optics Corporation 20600 Gramercy Place, Suite 103 Torrance, CA 90501	1
Dr. Hau–Kuang Liu JPL/Caltech Mail Stop 303–310 Pasadena, CA 91109–8099	1
Dr. Adolph W. Lohmann NEC 4 Independence Way Princeton, NJ 08540	1
Dr. Michael V. Morelli Texas Tech University Optical Systems Lab Department of Electrical Engineering Lubbock, TX 79409–4439	1
Dr. Dennis R. Pape Photonic Systems Inc. 1800 Penn St., Suite 4B Melbourne, FL 32901	1
Dr. Bernard H. Soffer Hughes Research Labs 3011 Malibu Canyon Road, RL 68 Malibu, CA 90265	1

	Copies
Dr. Wilfrid B. Veldkamp MIT Lincoln Labs 244 Wood St., L–270 Lexington, MA 02173	1
Mr. Carl Verber Georgia Institute of Technology Atlanta, GA 30307	1
Dr. John F. Walkup Texas Tech University Department of Electrical Engineering P. O. Box 4439 Lubbock, TX 79409–3102	1
Dr. Shudong Wu Pennsylvania State University Electrical Engineering Department University Park, PA 16802	1
Dr. Xiangyang Yang Pennsylvania State University Electrical Engineering Department University Park, PA 16802	1
Dr. Francis T. S. Yu Pennsylvania State University Electrical Engineering Department University Park, PA 16802	1
AMSMI-RD-CS-T	1
AMSMI-RD-CS-R	5
AMSMI-GC-IP, Fred Bush	1
AMSMI-RD, W. McCorkle	1
AMSMI-RD, R. Rhoades	1
AMSMI-RD-WS, W. Wharton	1
J. Bennett	1
S. Troglen	1
AMSMI–RD–WS–PO, James C. Kirsch	50
Don A. Gregory	1